ISSN 0016-8521, Geotectonics, 2023, Vol. 57, No. 6, pp. 693–725. © Pleiades Publishing, Ltd., 2023.
Russian Text © The Author(s), 2023, published in Geotektonika, 2023, No. 6, pp. 3–42.

The Pre-Quaternary Evolution of the Eurasia Basin: The Results of Interpretation of Seismic Profile ARC1407A

A. V. Zayonchek[a, *], S. Yu. Sokolov[a], and A. V. Soloviev[a, b]

[a] *Geological Institute, Russian Academy of Sciences, Moscow, 119017 Russia*

[b] *Russian Research Geological Petroleum Institute (VNIGNI), Moscow, 105118 Russia*

**e-mail: a_zayonchek@mail.ru*

Received April 18, 2023; revised September 21, 2023; accepted October 19, 2023

Abstract—This paper presents the results of a study of the pre-Quaternary tectonics and stratigraphy of the Eurasia Basin (EB) according to the interpretation of the ARC1407A seismic profile and calculations of the theoretical positions of linear magnetic anomalies. The sedimentary sequences are recognized in seismic profiles and their stratigraphic position is similar to that of sedimentary sequences in the western parts of the Nansen and Amundsen basins. The age indexation of sedimentary sequences corresponds to the ACEX drilling results and the main evolution stages of the EB. No previously recognized reference horizon with the age of ~34 Ma, which is related to the termination of spreading in the western part of North Atlantic and amalgamation of the Greenland and North American plates, is recognized, as is supported by our studies in the western parts of the EB. In the western part of the Nansen Basin we identified a reference horizon with the age of 38 Ma for the first time, which was previously traced in the western part of the Amundsen Basin, whose formation is related to the evolution stage of the Eurekan Orogen. A reference horizon with the age of ~26 Ma, which has been traced in the western part of the Amundsen Basin before, is also distinguished in the western part of the Nansen Basin within ARC1407A. This geological boundary is related to the beginning of unstable spreading in the western segment of the EB between the Yermak Plateau and Morris Jessup Rise (Plateau). The end of a long stratigraphic hiatus between 44.4 and 18.2 Ma in the section of ACEX boreholes is clearly correlated with the formation of a sedimentary sequence of ~19.6–18.3 Ma, which is the age of the beginning of the formation of a deep-water gateway between the North Atlantic and Eurasian sedimentary basins. This event coincides with the main reconstruction stage of movements of the Eurasia and North America plates, which led to a change in the direction of migration of momentary opening poles from the NNW to SSE. It is suggested that the thick sedimentary sequences in the Nansen Basin and the rift valley of the Gakkel Ridge that are observed in seismic section ARC1407A include Late Pliocene–Quaternary (<2.7 Ma) glaciomarine rocks, which compose a significant volume of sediments in the eastern part of the EB and the Gakkel Ridge.

Keywords: Arctic Ocean, Eurasia Basin, Gakkel Ridge, Amundsen Basin, Nansen Basin, spreading, geodynamics, linear magnetic anomalies, seismostratigraphy, sedimentary cover

DOI: 10.1134/S0016852123060080

INTRODUCTION

The Arctic Ocean includes two deep-water basins, Amerasia and Eurasia, divided by the Lomonosov Ridge. In contrast to the Amerasia Basin, whose geological evolution is still a matter of debate, the Eurasia Basin (EB) formed in the Cenozoic as a result of spreading between the North American and Eurasian plates in the opinion of most geologists and geophysicists [2, 9, 11, 12, 29, 30, 42, 55, 66, 86, 111] (Fig. 1). The EB contains a thick sedimentary cover in deep-water basins. The study of its structure was based on low-resolution data from drifting stations [14].

In 2001, the specialists from the Alfred Wegener Institute (AWI, Bremerhaven, Germany) provided the first qualitative seismic profiles for the EB, which allowed the systematic study of the sedimentary cover [79]. Since 2008, a significant volume of new seismic data within the EB has been produced in the framework of national programs of Russia, Norway, and Denmark [44, 56, 93].

The results of foreign studies are published in two summarizing works [44, 56], which used key German seismic profiles [79]. Various interpretation scenarios of domestic data are published in numerous works of three conditional groups: (i) the age of the continuous spreading of the EB is accepted as Cenozoic beginning from the Upper Paleocene [93], similar to foreign studies [44, 56, 79], (ii) the EB originated “long before the beginning of spreading postulated by magnetostratigraphy (~60–120 Ma before)” [6], and (iii) the evolution of spreading is limited only to the Eocene and Pliocene–Quaternary [22].

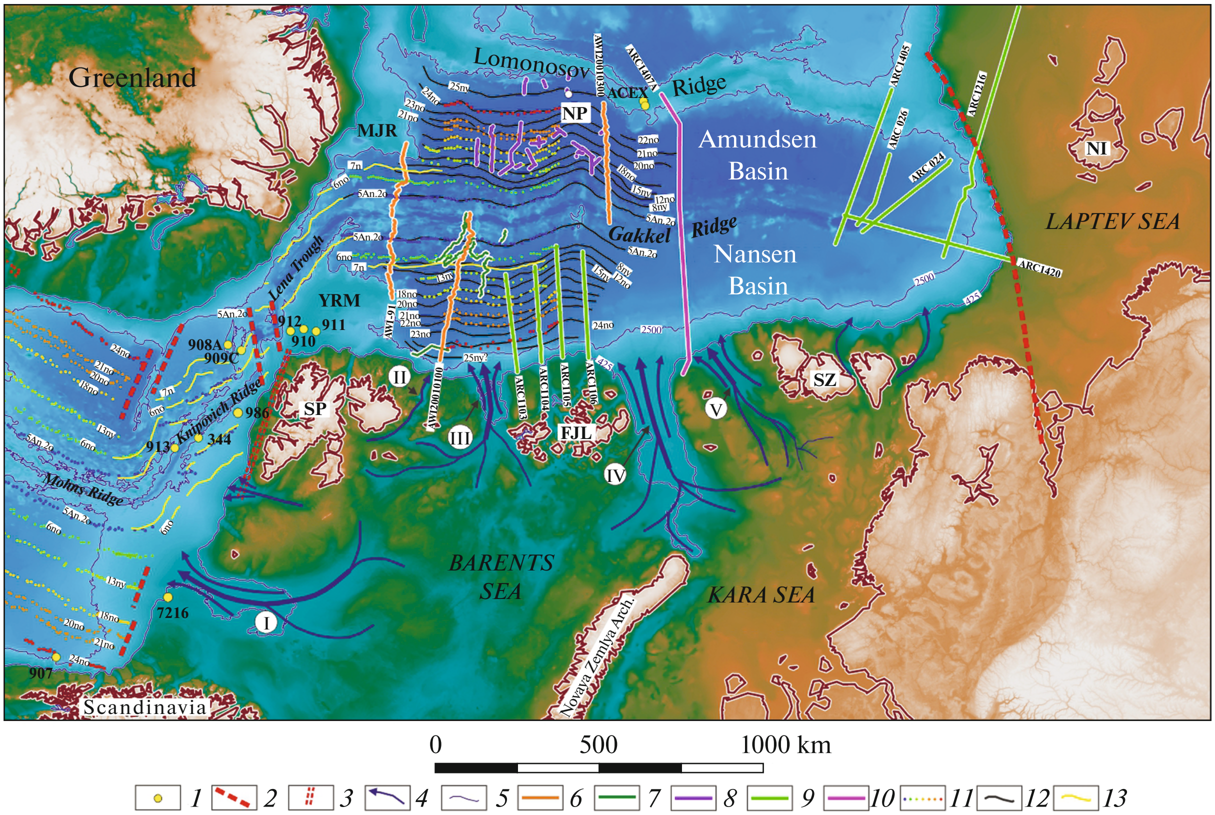

Fig. 1. The general bathymetric scheme of Eurasia Basin and the northern part of the Norwegian–Greenland Basin (Figs. 1, 2, 4–8 are based on the IBCAO v. 4 digital bathymetric model [77]). Here and in Figs. 2–4, 6, 8, and 11: NP, North Pole; SP, Spitsbergen Archipelago; FJL, Franz Josef Land; SZ, Severnaya Zemlya Archipelago; NI, Novosibirsk Islands; YRM, Yermak Plateau; MJR, Morris Jessup Rise. I, Medvezhinsky Trough; II, Eagle Trough; III, Franz-Victoria Trench; IV, St. Anna Trench; V, Voronin Trench. (*1*) Location of drilling boreholes; (*2*) main transform faults; (*3*) De Geer Megatransform Zone after [57, 58]; (*4*) main directions of runoff of glaciomarine sediments, modified after [31, 91]; (*5*) isobaths 425 and 2500 m; (*6–10*) position of seismic profiles: (*6*) AWI (Germany) after [44, 56, 79, 82]; (*7*) NPD (Norway) after [56]; (*8*) LOMROG (Denmark) after [44]; (*9*) ARC (Russia) after [9, 24, 93]; (*10*) ARC1407A (Russia) after [6, 22, 93]; (*11–13*) LMA axes: after [67] (*11*) [42] (*12*) and [55] (*13*).

Although we do not consider the ideas on the formation of the Eurasia sedimentary basin and elaborated models (after [6, 22]) in this work, because they contradict the geological–geophysical data on the evolution of the Eurasia sedimentary basin within the entire system of North Atlantic, the presence of sedimentary sequences of more than 500-m thick (locally, >1 km thick) within the central and eastern parts of the rift valley of the Gakkel Ridge [6, 20, 22, 79, 93, 105] requires explanation.

In addition, there are differences in seismostratigraphic models of the division of the EB sedimentary cover, which are based on ideas of continuous Cenozoic spreading. A key issue is related to the identification of a geological boundary with an age of ~34 Ma [93], which was missed by other researchers [9, 44, 56, 79] and requires verification.

Profile ARC1407A is the only one crossing the EB in its central part; it begins on a shelf of the Kara Sea (the western wall of the Voronin Trough), and ends in the Lomonosov Ridge 50 km from the location of the ACEX deep-water boreholes (Fig. 1). There are different interpretations of drilling results, one of which suggests the presence of a long stratigraphic hiatus of 44.4–18.2 Ma [36, 38, 60, 76], which is not supported by studies suggesting a short period of ~400 ka (within 36–34 Ma) [100], although both groups of researchers relate the end of the hiatus with the amalgamation of the North Atlantic and EB.

To resolve the contradictions in the interpretations of the age and the duration of the stratigraphic hiatus and thus the age indexation of the reference reflectors and the presence of thick sedimentary sequences in the rift valley of the Gakkel Ridge, we reinterpreted the key ARC1407A seismic profile. The extremely low quality of aeromagnetic data in the eastern part of the EB, however, keeps us from relying on the results of the identification of linear magnetic anomalies (LMAs) [2, 65, 93] in this sector of the basin; thus, we used two classical approaches, which are applied in the World Ocean areas without reliable magnetometric data.

The first approach is the verification of the corresponding geodynamic models and kinematic parameters of opening of tectonic plates. One of the elements includes plotting drift lines, which has been done in [2, 65, 93]. In this work, we made more detailed calculations of drift lines by momentary opening poles.

The second approach is the calculations of the position of theoretical LMAs (TLMAs) and thus the determination of the theoretical age of the oceanic crust [107].

THE INITIAL DATA AND ANALYTICAL METHODS

The basic technical characteristics (the length and the type of the receiving streamer, the number of channels, the tow depth, gun groups, sounding points, etc.) for ARC1407A and other seismic profiles (Fig. 1) were presented in [44, 56, 79, 82, 93]. In addition to seismic data, almost all regional works in the Arctic traditionally use the results of digital compilation of data: the IBCAO (International Bathymetric Chart of the Arctic Ocean) bathymetric results [77], CAMP-GM (Circum-Arctic Mapping Project – Gravity and Magnetic) magnitometry [63, 67], and DTU (Denmark Technical University) [33] or WGM (Word Gravity Map) [41] gravimetry projects. Because most scientific Arctic studies do not analyze the reliability of compilation data of the studied regions, we analyzed the quality of digital compilations of remote data for the EB and the northern part of the Norwegian–Greenland Basin.

Bathymetry

In this paper, we used the IBCAO v.4 digital relief model [77] without the Greenland Ice Sheet. The resolution of the model is 200 × 200 m, which became possible due to the use of multibeam echo-sounder (MES) data. Significant areas of the continental slope of the western part of the Barents Sea, the adjacent areas of deep water basins, the Knipovich Ridge, and the northern part of the Mohns Ridge are covered by MES data with the size of initial survey grids of 50 × 50 or 100 × 100 m. In this area, the precision and detail of IBCAO v.4 [77] are maximal. In the EB, the compilation included individual MES profiles, which partly spanned the rift valley of the Gakkel Ridge, some areas of adjacent deep water basins, and the slope of the Lomonosov Ridge (Fig. 2).

For most MES-free water areas, we traditionally used the results of profile measurement and digital navigation and other compilation maps. The resolution of primary navigation maps significantly varies. The precision and the resolution of data within the western margin of the Barents Sea and adjacent deep-water basins is significantly higher than for the Russian northern sector of the Barents–Kara margin.

These IBCAO v.4 [77] compilation parameters also significantly differ for various areas of the EB. They generally do not correspond to the grid resolution of 200 × 200 m because of the varying density of data at a uniform grid step. In addition, the junction areas of small- and large-scale data inevitably contain "artifacts" in the form of various transformants, especially, in areas with low relief gradient. All these peculiarities should be taken into account in the interpretation of the data.

Gravimetry

The results of the WGM-2012 project [41] were used in this study as a gravimetric basis. With respect to the equatorial Atlantic, the models of free air gravity anomalies used the results of the DTU10 project (Lyngby, Denmark) with a grid-cell size of 1′ × 1′ [33]. In this project, as in other analogs, the initial data for deep-water marine areas include the results of satellite altimetry observations, which were recalculated to gravity anomalies, although this technology has some limitations, which have been considered by geodesists in detail [39, 103].

The following is important for geological interpretation in the Arctic region. The method uses complex summarizing and filtration algorithms for initial altimetry data along the lines of satellite tracks. The filtration window is 25–30 km for data from the ERS-1 (1991), ERS-2 (1995), and ICESat (2003) satellites, which were used in modeling prior to the DTU-10 results [33].

This means that the anomalous gravity signal from the rift valleys and near-rift seamounts, transform and nontransform faults, continental slopes, and lower order structures fall into the filtration window and the anomalous gravity field from these objects partly loses intensity and becomes smoothed. In the Arctic, the signal distortion upon the reflection from the ice surface is the main source of errors of altimetry observations.

Various Arctic areas are unevenly covered by ice and the observation errors vary depending on the region. The external quality control is conducted from independent sources. The ice-covered Arctic water area was mapped by various surveys: from submarine and surface devices, using ice- and airborne measurements. In each survey type, the resulting data have certain limitations and errors, thus it is impossible to conduct a correct analysis of the precision and filtration characteristics of altimetry observations.

We can however use the results of comparison (DTU8 project [34]) for deep-water and shelf areas around the Spitsbergen Archipelago and North Greenland, which belong to the ice type (ice-covered Arctic water areas) according to geodetic altimetry.

The reason for the choice of this area as a reference is deliberate because of the significant volume of marine and airborne gravimetric surveys during the

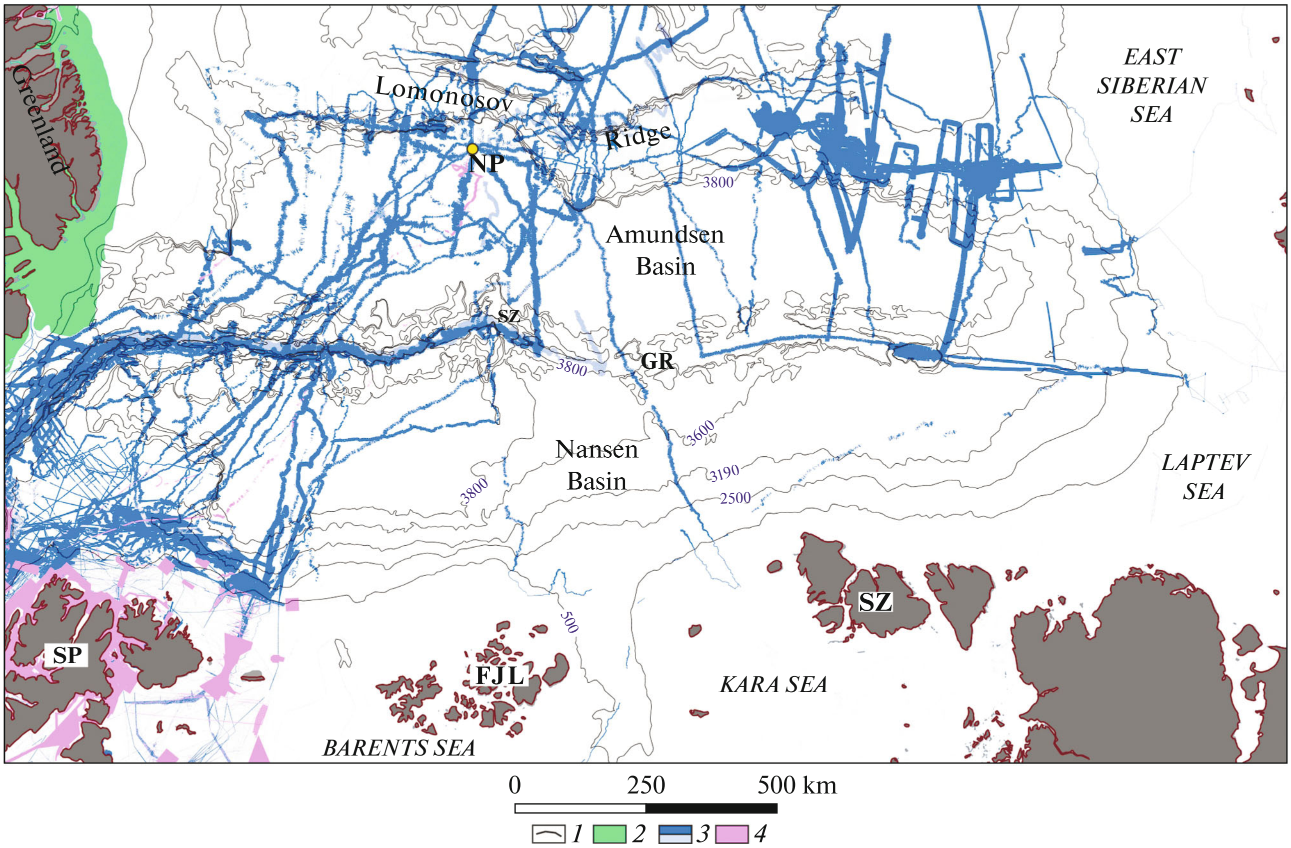

Fig. 2. The scheme of high-resolution bathymetric studies of the Eurasia Basin and adjacent water areas. NP, North Pole; GR, Gakkel Ridge; SP, Spitsbergen Archipelago; FJL, Franz Josef Land; SZ, Severnaya Zemlya Archipelago. (*1*) Isobaths 500, 2500, 3190, 3600, and 3800 m; *2–4*, data: (*2*) compilation for Greenland shelf; (*3*) multibeam echo-sounding; (*4*) high-resolution multibeam echo-sounding.

ArcGP project [59]. It is necessary to understand that marine gravimetric observations have certain errors in their medium- and long-wavelength components, which are related to nonlinear sliding of the zero point of a marine gravimeter during long cruise "shoulders." For this Arctic area, nonlinear sliding was taken into account very correctly, because of the close presence of a reference gravimetric point on the Spitsbergen Archipelago, which allowed frequent timewise gravimetric surveys in the ArcGP project [59]. A technological peculiarity of airborne gravimetry is related to the application of a timewise filtration algorithm to primary data. The filtration window is 20–25 km (depending on the speed of the aircraft); this is lower than that in satellite altimetry. The comparison of the DTU8 [34] and ArcGP [59] projects showed a standard average statistical deviation of 5.8 mGal at the maximum value of 34.4 mGal [34, 35].

The region to be compared (shelves around the Spitsbergen Archipelago and North Greenland, adjacent areas of the EB) has contrasting tectonic structures: ridges, transform faults, continental margins, rises, slopes, and basins, which exhibit striking high-frequency gravity anomalies.

The results feasibly reflect the altimetry loss of the high-frequency signal part in ice conditions, but the airborne gravimetry data can also have significant errors within individual profile areas. These errors are typically caused by hitting turbulence in the aircraft, which leads to the destabilization of gravimeters and a sharp loss of precision. Depending on the intensity and duration of the turbulence pulse, the gravimeter returns back to the operating regime in 1–30 min, which is equivalent to distances of 6.7–200 km at an average speed of the aircraft of 400 km/h.

As an example, we can compare the NRL-98/99 airborne gravimetry data (an interprofile distance of 18–20 km) [42] and the data that resulted from the LOMGRV-09 project (an interprofile distance of 10–15 km) [49] in the shelf area of the continental slope of Greenland and North America, Lomonosov and Alpha ridges, and adjacent deep-water basins. The results of the analysis in the interception points of profiles show that the difference is less than 5 mGal at the maximum values of more than 15 mGal. The comparison of the NRL data with ice surface gravimetry observations from national databases of Canada and Denmark showed the presence of local extreme errors of up to ~80 mGal [50].

A new generation of low-orbital Jason-1 and -2, Cryosat-2, and Saral-AltiKa satellites was launched in 2011–2013 allowing a significant increase in the high-frequency component of altimetry measurements. As a result, a refined DTU13 gravity field model of the Arctic water area (a cell size of $1' \times 1'$) was made at the Denmark Space Research Institute (Lyngby, Denmark), which allowed the Nordic Geoscience Pty. Ltd. company (Melbourne, Australia) to conduct additional processing of primary altimetry measurements and to produce a refined NORDIC13 digital model (a cell size of $1' \times 1'$), which spans the area of the Arctic Ocean between 65° and 88° N [46, 47]. For the ice-free shelf areas, the error of the refined model is 1.0–2.0 mGal [46, 47]; however, the real errors and filtration window for deep-water ice-covered Arctic remain problematic.

New estimations of the precision of the filtration values of altimetry gravimetric compilations are expected, which is related to numerous marine observations in 2004–2014 in the Canadian Basin within the framework of national programs of the United States and Canada on the determination of the outer continental shelf boundary (OCSB). The execution of the Russian OCSB program was accompanied by gravimetric observations for some seismic profiles; however, their fragmentation and single interception points prevent objective comparison.

In this study, we used the digital Bouguer gravity field models of the WGM201 project and an isostatic model calculated from the Airi–Heiskanen model [39].

Magnetometry

The results of the CAMP-GM project [63, 67] are traditionally used as a magnetometric base. The matrix has a grid cell size of 2 × 2 km, but the values are recalculated to the upper semispace at a height of 1 km.

For the magnetic field, the project is based on the combined compilations of national digital anomalous magnetic anomaly field (MAF) matrices, which were made by specialists from Russia (Russian Research Geological Institute (VSEGEI) and VNIIOkeangeologia, St. Petersburg), the United States (United States Geological Survey, USGS), Canada (Geological Survey of Canada, GSC), Norway (Norwegian Geological Survey, NGU), Sweden (Sweden Geological Survey, SGS), Denmark (Geological Survey of Denmark and Greenland, GEUS), and Finland (Geological Survey of Finland, GTK).

The task of combining surveys of various scales, heights, directions, and measurement and navigation precision, which have been conducted from the 1960s to the present in Arctic with severe climate and intense variations and the displacement of the magnetic pole, is extremely difficult. The technical description of the results of the CAMP-GM project is poor and prevents strict mathematic analysis of the quality of the free matrix.

The initial national matrices have different cell sizes: 1 × 1 km in most foreign compilations, 2 × 2 km in the North Atlantic, and $3' \times 3'$ with recalculation of the field to the upper semispace at a height of 5 km for the western Greenland. Because the matrix step of the CAMP-GM project is 2 × 2 km, the foreign matrices (excluding western Greenland) have excessive or equal densities in the resulting compilations. The domestic digital compilations (VSEGEI and VNIIOkeangeologia) have significantly lower of matrix resolutions and the cell size is only 5 × 5 km. This means that for the coverage area of domestic matrices, which is less than 50% of the area, the announced aim (on digital maps at a scale of 1 : 5000000) is not achieved, because, in this case, the minimum step of the grid cell must be 2.5 × 2.5 km (at a commonly accepted standard, the level of detail of the matrix must be at least two times higher than the map scale).

According to the technical description of the CAMP-GM project [66], the combined VSEGEI matrix was recalculated to the upper semispace at a height of 5 km, which narrows its range during interpretation. This is related to the depth of the magnetically active oceanic basement.

In accordance with seismic data, the basement in the central parts of the Amundsen and Nansen basins occurs at depths of 6–8 km (e.g., [93]). If we take the average value (7 km) and add the average flight height during the airborne survey of 0.4 km and the recalculated height of 5 km, the value will be 12.4 km. It is evident that at this geological and technical altitude, the MAF medium-wavelength component would be strongly smoothed, the intensity will sharply decrease, and many local anomalies will disappear or change their morphologies and axes as a result of joining. In fact, the VSEGEI matrix for the water basins can be considered a small-scale digital scheme rather than a digital map.

According to the technical description of the CAMP-GM project [66], the combined VNIIOkeangeologiya matrix was not recalculated to the upper semispace. For the EB, the MAF matrices are significantly overlapped and the VNIIOkeangeologiya matrix completely spans the entire EB (Fig. 3).

Because this initial matrix was not recalculated to the upper semispace, it is logical to use this matrix in the CAMP-GM compilation for the EB. Since the technical project description does not analyze the initial data and methods of their processing and linkage, we were guided by publications on the combined geophysical data prepared by specialists of VNIIOkeangeologiya [2, 87] and joint publications of specialists of the Naval Research Laboratory (NRL, Research Laboratory of the United States Navy) and VNIIOkeangeologiya [72, 85]. The publication of 2018 [3] prepared by specialists of VNIIOkeangeologiya summa-

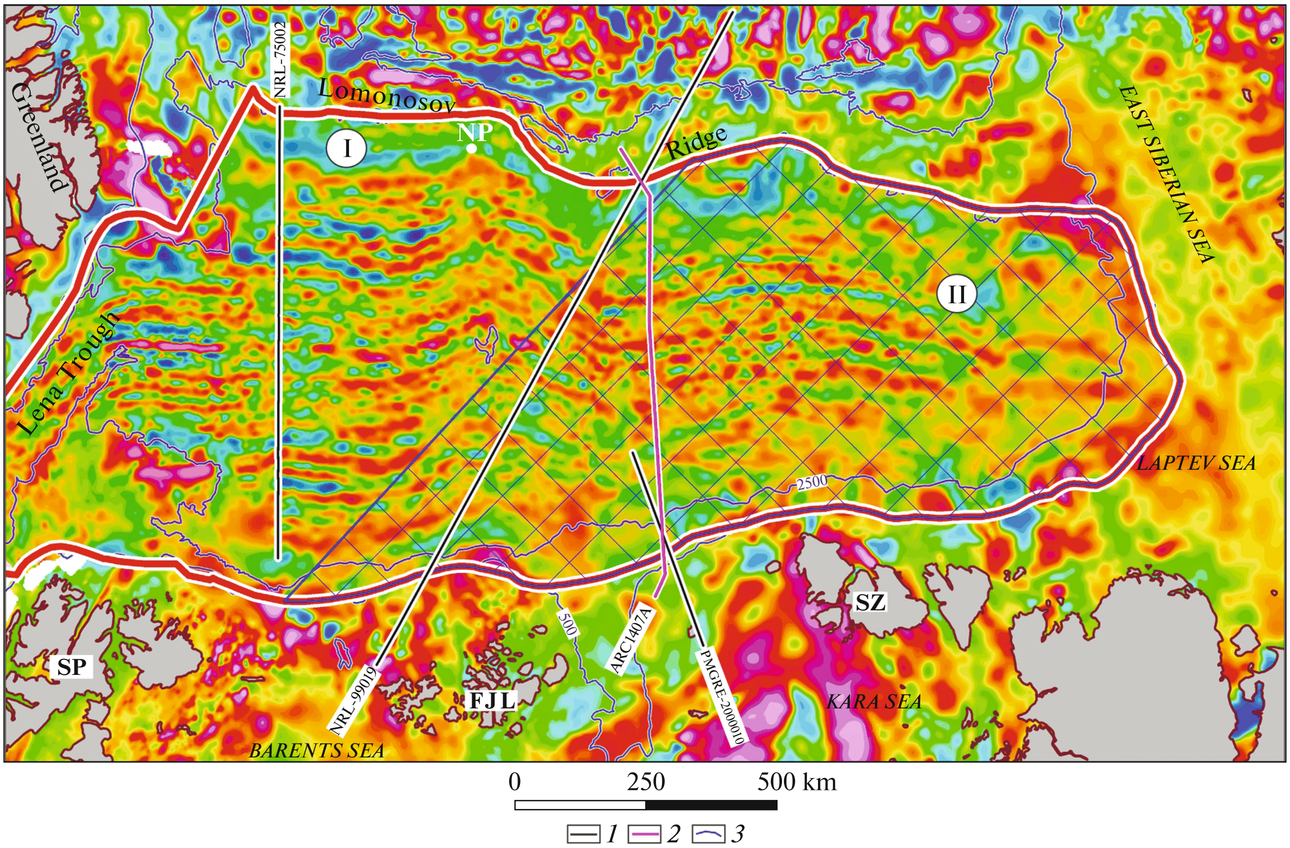

Fig. 3. The contours of domestic digital MAF models (grids of 5 × 5 km) used for the Eurasia Basin during the compilation in CAMP-GM project after [63, 67] (based on the digital MAF model of the CAMP-GM project after [63, 67]). NP, North Pole; SP, Spitsbergen Archipelago; FJL, Franz Josef Land; SZ, Severnaya Zemlya Archipelago. Contours of domestic digital MAF models: I, VNIIOkeangeologiya (dark areas); II, VSEGEI (hatching). (*1*) Position of analyzed aeromagnetic profiles (the results are given in Fig. 5); (*2*) position of seismic profile ARC1407A after [6, 22, 93]; (*3*) isobaths of 500 and 2500 m.

rizes the results of domestic gravimagnetic studies of the Arctic Ocean.

In contrast to the previous works, in which the researchers were forced to rely mostly on data from primary materials during the analysis of domestic magnetometric data of various ages, [3] analyzed historical airborne surveys in comparison with modern information (airborne and marine surveys). It was established that the regional domestic surveys of 1961–1978 are characterized by positioning errors from ±570 to ±38000 m.

During the works, the researchers compared the domestic data relying on new surveys that partly cover the Arctic seas of Russia and cover the adjacent deep-water basins insignificantly. We fully support the opinion that the results of these surveys are a reconnaissance and give only a general idea on the MAF structure of the studied regions and thus are unsuitable even for research targets larger than at a scale of 1 : 2500000 [3].

At the same time, the magnetometric studies of the American specialists and possibility of the correlation of their historical data dramatically differ from the results of studies of Russian specialists. All of the conditionally "western" EB part is covered by two regular airborne gravimetric NRL surveys of 1998–1999 (Fig. 4).

The survey was conducted with the highest-precision GPS navigation for that period (<1 m for three components) [41]. The survey data have significant peculiarities related to their task: the measurement of gravimetric data (accompanied by magnetometric survey) for the composing a maximally precise Arctic digital model of free-air gravity field anomalies. This was a geodetic task for composing a refined geoid model, which is suitable for launching the new generation of low-orbit satellites (TV communication, weather, etc.), as was successfully implemented within the ArcGP international project [57].

Judging from this task, the technical survey parameters were chosen taking into account the scale of the Arctic water areas and necessary (geodetic) frequency characteristics: medium- and long-wavelength gravity field components. The survey parameters (an interprofile distance of 18–20 km, an average flight height of 600 m, and an average flight speed of 465 km/h) [42] thus significantly differ from the parameters accepted

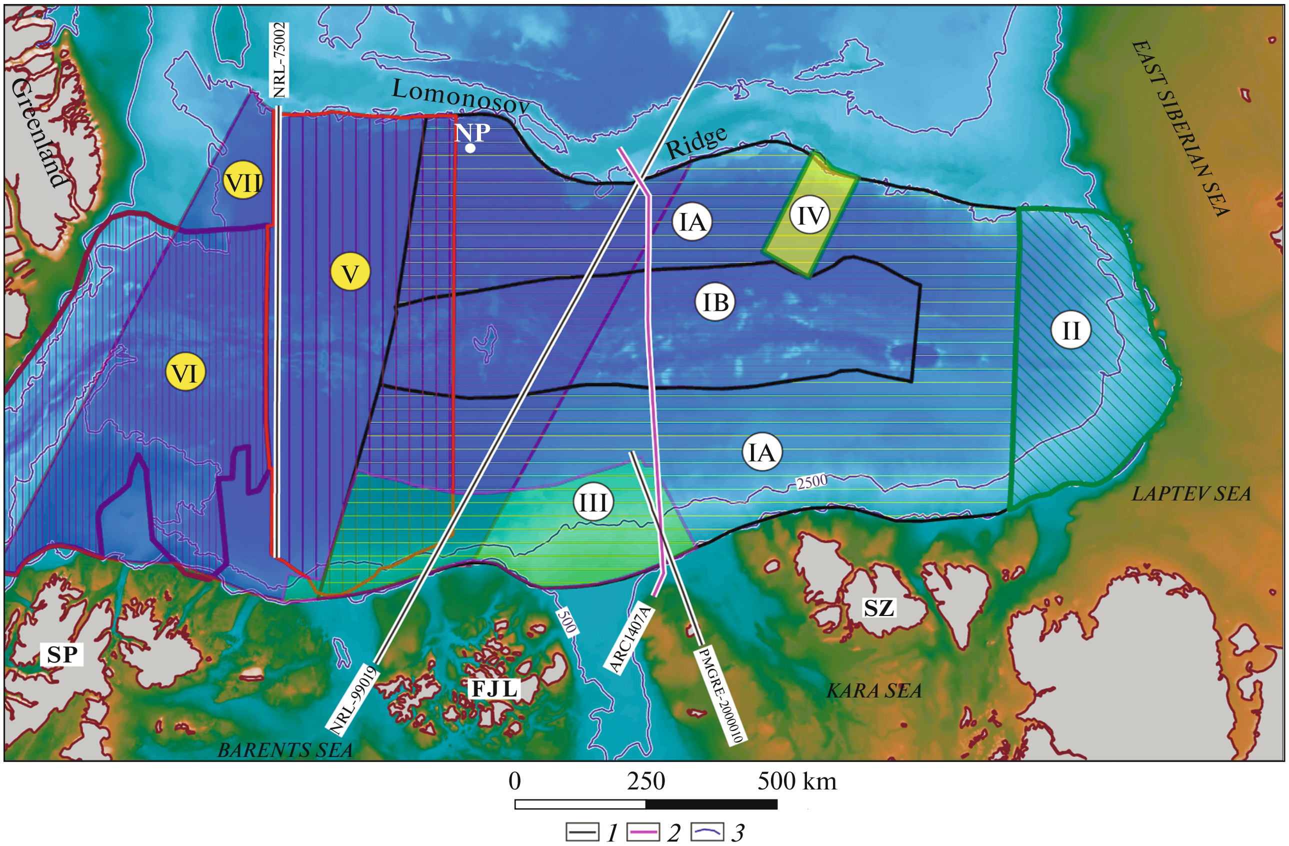

Fig. 4. A map of magnetometric studies and profile density of observation network in the Eurasia Basin. NP, North Pole; SP, Spitsbergen Archipelago; FJL, Franz Josef Land; SZ, Severnaya Zemlya Archipelago. Contours of aeromagnetic surveys (IA, IB–IV, Russian Federation; V–VII, United States, Russian Federation) by interprofile distance and years of studies: IA, ~8–10 km (1965–1966); IB, ~25–40 km (1968–1969); II, ~25 km (1973); III, 10 km (1993, 1998, 1999, and 2000); IV, 5 km (1992); V, ~8–16 km (NRL-75, 1975); VI, ~8 km (NRL-73, NRL-74, 1973–1974); VII, ~18–20 km (NRL-98, NRL-99, 1998–1999), contour is darker; (*1*) aeromagnetic profiles (Fig. 5); (*2*) seismic profile ARC1407A (Russian Federation) after [6, 22, 93]; (*3*) isobaths 500 and 2500 m.

in a geodetic survey. The average flight height of the aircraft for a regional magnetometric survey is 350–400 m at a speed of 300–350 km/h.

In addition, the surveys of 1998–1999 for the western part of the EB were conducted at an angle of ∟40° to the direction of the ridge strike rather than transversely (Fig. 4). The magnetometric information is thus smoothed relatively to the NRL surveys of 1973–1975 (Fig. 5).

At the same time, the systematics, the high precision of the NRL survey navigation in 1998 and 1999, and the interception of old surveys at an angle (significant volumes of interception points necessary for the analysis of quality of data and correlation) allowed the full identification and correction of navigation errors in old surveys [85].

In their precision the historical magnetometric surveys can conditionally be divided into several classes, which are directly related to the possibilities of instrumental measurements. The most important real navigation parameters of the historical surveys include their internal and external navigation errors. The radio navigation stations placed along the perimeter of the survey boundaries (on land, islands, or drifting ice) yielded positioning errors and the total precision of the polygon positioning mainly depended on the distance from stations (external positioning). If the number of radio navigation stations was sufficient and they were placed maximally close to the survey perimeter, the equipment operated stably, and the weather conditions during the flights were good, the internal positioning could be higher than the external one. These are extremely important parameters, which affect the possibility of correlation of historical and modern data.

The surveys of the 1960s (until 1970, inclusively) belong to the lowest precision class. Because of the imperfect radio navigation equipment of those years and a weak radio signal, the parameters of these surveys belong to the navigation–radiogeodetic positioning class. The remoteness of some profile areas from weak basic navigation stations within these areas (segments) resulted in areas of radio signal loss.

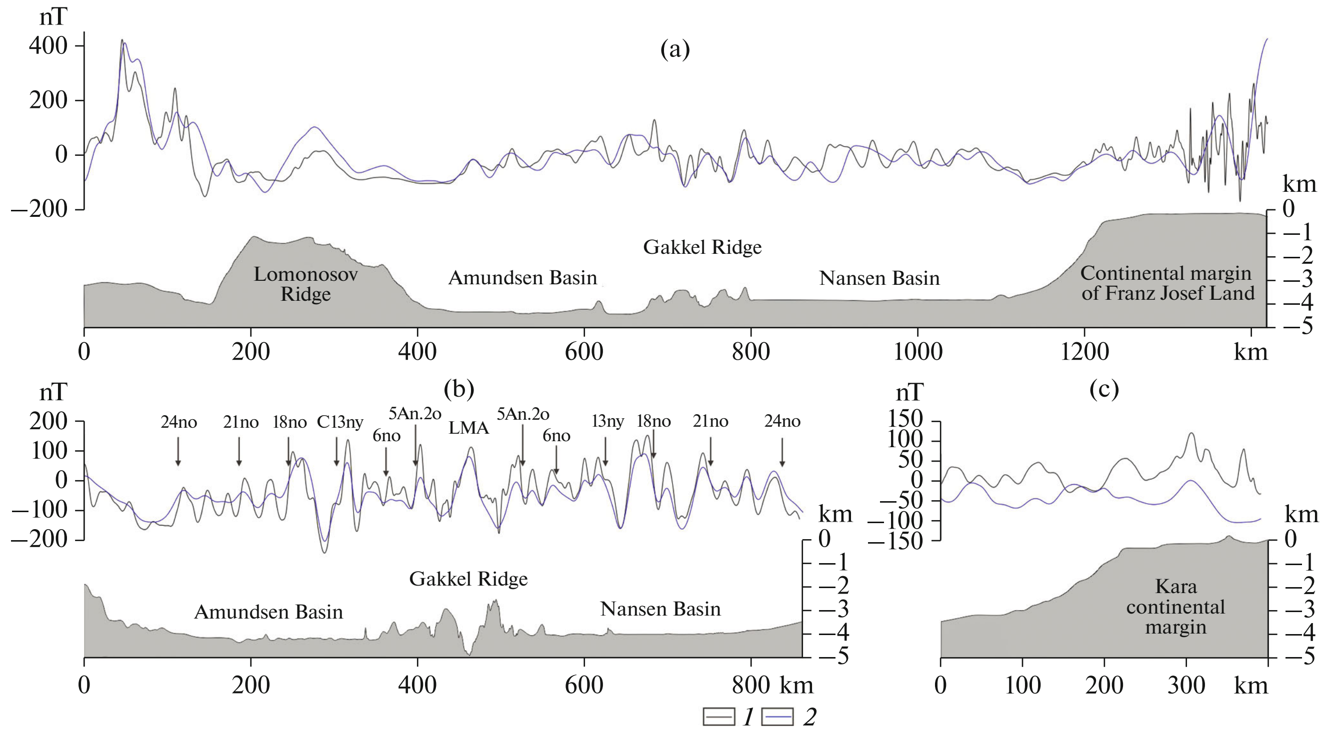

Fig. 5. Comparison of the observed MAF curves with those extracted from digital AMF model of the CAMP-GM project [63, 67, 77] along the lines of aeromagnetic profiles (for the position, see Fig. 3, drift line 4). The topography is extracted from the IBCAO v.4 digital bathymetric model [77]. a–c, profiles: a, NRL-75002; b, NRL-99019; c, PMGE-2000010. LMA (5An.2o–24no), position of identified LMAs after [9]. *1*, *2*, MAF curves: (*1*) observed; (*2*) extracted from CAMP-GM digital model after [63, 67].

In this case, the navigation for these segments was carried out by piloting. The specialists who participated in field works onboard the aircraft were aware of unpredictable Arctic winds at low flight echelons. In the beginning of the flight along the profile line at constant engine power parameters, the ground speed could be 350 km/h reaching 370 km/h in the middle of the profile line and decreasing to 330 km/h at the end of the profile. These flight changes are also possible for shifts relative to the axial line of the profile depending on the wind direction. All this is well determined using GPS navigation in contrast to the averaged ground piloting values, which were applied in past periods with the use of unstable radio navigation for the areas of signal loss by basic stations (no visual or photo positioning occurred during the work above the Arctic water area).

This means that nonlinear navigation errors are present within single profiles. These issues are manifested in the following: the absence of the parallel profiles, different interprofile distances, and individual profile segments with a typical course change. These surveys have extremely low external and internal navigation characteristics. All these disadvantages were typical of domestic surveys of the 1960s, which were conducted in the eastern part of the EB (Fig. 4).

In addition, the level of detail of data of the studies was 8–10 and 25–40 km directly above the Gakkel Ridge and for the deep-water basins, respectively, which significantly decreases the informativity of the field. Because of these peculiarities, which present nonlinear errors inside the profile, it is almost impossible to precisely analyze the navigation errors; maximum navigation errors of up to 38000 km are possible for them [3] and these data can only be used as a small-scale scheme for visual analysis. These data reflect the difficulties of navigation that were met by the first Arctic researchers during airborne surveys.

Data Comparison

In 1948, Soviet researchers began annual and systematic studies of the Arctic seafloor in the framework of high-latitude air expeditions; in 1950 they continued geological–geophysical studies from the "Northern Pole" drifting research stations.

In 1948, a group of geologists of a scientific expedition from the Research Institute of Arctic Geology, Academy of Sciences, USSR under the leadership of Ya.Ya. Gakkel discovered the Lomonosov Ridge. Gakkel first proposed the continuation of a submarine volcanic mid-oceanic ridge from the northern part of the Atlantic Ocean to the Eurasian part of the Arctic

Basin, which was further named in his honor [15]. The existence of this ridge was fully confirmed by hydrographic and geophysical studies [7, 15]. At the beginning of aerogeophysical works under the leadership of A.M. Karasik (Research Institute of Arctic Geology, Academy of Sciences, USSR), the first Arctic seafloor bathymetric maps were composed by a hydrographic survey of the Soviet Union Navy, which became the basis for the Geomorphological Map of the Arctic Ocean composed by Dibner et al. [8].

In the general plan of the eastern part of the EB (the area of the most extensive Soviet Union studies), the position of the Gakkel Ridge was clearly identified prior to 1965 [8]. Further airborne surveys were aimed at detailed works exactly above the ridge. The navigation precision prevents the symmetric study of ridge flanks that characterize the possibilities of external positioning (Fig. 4).

The surveys of 1971–1972 could conditionally be called transitional. It is evident that the radio navigation equipment was probably perfected due to intensification of the radio signal from basic stations, thus the areas of its loss within single profiles was strongly reduced. The surveys of this class for the EB are absent. The NRL survey (United States) of 1972 conducted above the Mohns Ridge, its flanks, and adjacent basins is a typical survey of this transitional class. The parallel character of the profiles and the interprofile distance became more stable. The single profiles, however, contain areas of a sharp course change, which is evidently related to radio signal loss from basic stations and attempts by the aircraft crew to find the signal. It is likely that the internal navigation precision was 0.5–2 km with maximum jumps of up to 3–4 km, but it contains sharp changes within single profiles.

The surveys conducted beginning from 1973 and, especially, from 1974 belong to a new class with higher stability of flight directions and parallel profiles indicating significant perfection of the radio navigation equipment. This survey class (NRL-1973, NRL-1974, and NRL-1975) covers the western part of the EB. The average interprofile distance for the NRL surveys is ~8 km for 1973–1974, ~8 km for some area in 1975, and ~16 km for the rest of the area in 1973–1975. Better internal (rather than external) navigation errors are a typical feature of these surveys. Based on the modern data of 1989–1999, it was therefore possible to define the external survey error and correct the navigation [85], as well to use the entire data array (historical and modern), which significantly affected the level of detail of the MAF digital model and the quality of the identification of the LMA axes [42].

Extraction of values along the lines of the observed aeromagnetic profiles from the matrix and visual comparison with MAF plots is the only method of verification of the correctness of the matrix of the Camp-GM project [63, 67]. We thus chose three aeromagnetic profiles with the ability to provide a general idea of various EB areas (Figs. 3, 5):

— profile NRL-75002 (United States, 1975) of the MAF of the western part of the EB with the highest spreading rates at the maximum density of well-positioned NRL data (Fig. 5a);

— profile NRL-99019 (United States, 1999, high-precise GPS navigation) of the MAF of the central part of the EB in the interception area with the historical materials of Soviet expeditions [11] (Fig. 5b);

— profile PMGE-2000010 (Russian Federation, 2000, GPS navigation, survey at a scale of 1 : 1000000 within the program of the State Geological Mapping of the Russian Federation), which intersects the ARC1407A seismic profile in the area of the continental slope and the area of the lowest quality of historical materials of the Soviet expeditions (Fig. 5c).

Profile NRL-75002 has a different frequency range, which was observed and extracted from the MAF matrix (Fig. 5a). The smoothed character of the field from the matrix is due to an insufficient grid cell size of 5 × 5 km. The high-frequency MAF part above the Gakkel Ridge is completely lost, whereas from 15 to 100% of the amplitude of the medium-wavelength part is lost. At the same time, all LMAs are identified, although some profile areas exhibit insignificant shifts, which are caused by averaging at grids of 5 × 5 km and further recalculation in the upper semispace at a height of 1 km.

Some areas of profile NRL-99019 exhibit an opposite phase of the observed and extracted fields in addition to complete loss of the high-frequency component in the area of the continental margin of the Franz Josef Land Archipelago (FJLA) and a partial loss of the medium-wavelength component (Fig. 5a).

Profile PMGE-2000010 from the shelf edge is characterized by totally inconsistent fields (Fig. 5c). The causes of the data discrepancy are numerous, although the absence of a proper technical description of the CAMP-GM project [63, 67] makes this issue difficult. The CAMP-GM project is a result of the combination of various matrices. There are various algorithms of this combination, but each algorithm requires the interception area of matrices and the priority of one matrix above the other in the interception area. The most likely reasons for unallowable differences between the initial profile MAF curves and curves extracted from the matrix could be:

— VNIIOkeangeologiya and VSEGEI matrices were combined in the central part of the EB yielding errors at the combination stage due to the different frequency ranges (the recalculation of the VSEGEI AMF matrix to the upper semispace for the height of 5 km);

— during the combination of the VNIIOkeangeologiya matrices of single surveys, priority was given to the matrix that was calculated from less qualitative data of the 1960s rather than matrices calculated from the results of the most precise and informative NRL or PMGE surveys.

The precise reasons for these differences are not important due to the absence of aeromagnetic MAF data suitable for the qualitative visual and quantitative modern interpretation for the entire eastern sector of the EB, including the ARC1407A seismic profile and all other profiles located to the east up to the Laptev Sea. It is impossible to correctly identify the LMA axes in the eastern part of the EB, which does not allow the perfection of the results of the work of Glebovitsky et al. [2].

A further full study of the tectonic evolution of this Arctic segment will require new aerogeophysical surveys. Two local areas in the Amundsen and Nansen basins covered by PMGE surveys using GPS navigation prevent reliable refinements because of the ultraslow rates of spreading in the eastern sector, which occurred over the last tens of millions of years. Reliable LMA identification needs a reference point: the magnetic field above the Gakkel Ridge (Fig. 4).

The extremely low spreading rate during the formation of C13 in the EB [2] results in a strong superposition of fields and the MAF above the area of the oceanic crust, which formed during its underplating, and is most often a local complication rather than a local anomaly, as in North Atlantic. This is shown by aeromagnetic profile PR75002 located in the west of the EB, where the spreading rates are maximal (the best LMA contrast) (Fig. 5b).

Detailed consideration of aeromagnetic data reveals a trend of gradual attenuation and further disappearance of this complication on the MAF curves toward the east. Therefore, LMA 13 was not identified in the EB by American researchers [42].

Single traces of MAF complication in the LMA 13 area can be seen in NRL-1999 profiles located in the central part of the EB in front of the FJLA. Further to the east, the anomaly is completely lost, which is related to the decrease in the spreading rate. In works on LMA identification or using of results of identification [2, 93] in the EB eastern sector, LMA 13 is positioned in the center of a negative anomaly, which, as suggested, divides the anomaly groups from C7–12 and C15–18. This is a suggested LMA 13 position rather than its identified position according to AMF data, which leads to the impossibility of orientation on this position during geodynamic or seismostratigraphic analysis.

Another complicating factor of the Nansen Basin for LMA identification is related to a significant deepening of the magnetoactive basement (oceanic crust) because of the thick sedimentary cover, which leads to a significantly smoothed MAF.

Judging from the analysis and comparison of data, we can state that the retrospective domestic data in the eastern part of the EB are unreliable for LMA identification. There are local areas at the flanks of the Gakkel Ridge to approximately LMA 6n (~19.6 Ma) in the Amundsen Basin that are covered by detailed retrospective aeromagnetic surveys, where the precision of the identification is significantly higher, but correct analysis of the precision of the LMA identification in these areas is impossible (Fig. 4).

It is evident that the inconsistency of present-day spreading axes and paleoaxes of the period of 53.9–33 Ma in the western part of the EB [2] should also occur in its eastern part. Closer to the continental margin of the Laptev Sea, the time period of instability should be similar to 33–0 Ma, which is caused by the close location of spreading poles. Correct regional zoning (long-lived segmentation) is impossible because of the thick sedimentary cover and because the seismic data in the eastern part of the Nansen Basin are almost absent, which also makes the recognition of symmetric segments in the basins relative to the present-day spreading axis impossible.

RESULTS

The analysis of the results of gravimetric studies confirms the ideas of Glebovitsky et al. [3] that the potential fields of both the deep-water part of the Arctic Ocean and the entire part of the adjacent Russian shelf are still poorly studied. As well, the quality and the detail of Arctic magnetometric data are the worst for most areas of the deep-water part of the Arctic Ocean adjacent to the marginal seas of the Russian Arctic.

In contrast to the foreign studies, the focus of domestic works of recent decades was shifted toward seismic works. At the same time, only one shallow borehole was drilled in the deep-water part of the Arctic in the Lomonosov Ridge and no further drilling in deep-water basins is expected in the nearest future. The interpretation of seismic data would thus more or less rely on tectonic reconstructions, which cannot be perfected without modern magnetometric information.

In contrast to the suggestion of Glebovitsky et al. [3], we do not consider that the results of satellite altimetry within the ice-covered part of the Arctic will reach the precision level to be compared with regional gravimetric surveys soon. It is obvious that the new generation of low-orbit satellites allows the registration of the higher-frequency part of the gravity field, but the wave reflection from the ice cover has no systematic class, because it depends on numerous complex factors: the thickness of the ice cover, hummocking, maturity and contamination of the ice cover (different reflection coefficients), the presence and sizes of polynyas, etc.

It is evident that during further aerogeophysical works aeromagnetometric studies should be prioritized and accompanied by aerogravimetry. We are sure that the organization of new aeromagnetometric expeditions in the deep-water part of the Arctic Ocean will provide optimal solutions: sufficient flight safety, planning profiles to obtain the maximum amount of geological data, and uncompromising variation control.

THE TECTONICS OF THE STUDIED REGION

The Geodynamic Setting

A present-day divergent boundary between the EB and North American Plate occurs within all of North America from the Newfoundland–Iberian segment and continues in the EB of the Arctic Ocean [25, 66, 106]. The deep-water EB formed in the Cenozoic as a result of slow (transiting to ultraslow) spreading of the North American (including the Lomonosov Ridge) and Eurasian plates [2, 9, 11, 12, 29, 30, 42, 55, 66, 86, 89, 111] (Fig. 1).

Because various scales of inversion of the geomagnetic field were used for the LMA identification, the age indexation in this work is given according to the International Geologic Time Scale of 2020 (GTS 2020) [74], which contains the scale of inversions of the geomagnetic field [98].

There are some differences in LMA correlation with geomagnetic polarity chrons (further, chrons) and their naming. At this study, we accepted the modern style, which means that the LMAs in the Northern Hemisphere belong to an interval of direct polarity of one chron or subchron (n, normal) and are divided at the age of its formation (o, old) and/or end (y, young). In other studies, LMA (or its part) identification followed the center of positive magnetic anomalies [2, 55]; therefore, they are depicted as meaning the center of the direct polarity chron. The chrons, subchrons, LMAs, theoretical LMA (TLMA) axes, finite rotation poles (further, poles), and position of the TMLA points on the rift lines are systematized in Table 1.

The present-day segmentation of the Gakkel Ridge has been reviewed in numerous works [54, 90, 93]. Because in this work we consider some features of the structure of sedimentary cover, we decided to divide the EB into western and eastern parts; the conditional boundary between them correspond to drift line 5 and the middle of the line coincides with the maximum curve of the Gakkel Ridge in its central part (Fig. 6).

During the Eocene–Early Oligocene (LMA C24no–13ny, 53.9–33.2 Ma), the EB evolved independently from the North Atlantic because of the presence of the Greenland Plate [2, 42, 62, 66]. In the northern part of the Norwegian–Greenland Basin, transform movement of Greenland occurred relative to the western margin of the Barents Sea along the De-Geer Megatransform Zone [55, 57, 58].

In this period, none of the EB segments could be considered Atlantic from a geodynamic viewpoint. Before the beginning of the EB spreading, the Lomonosov Ridge was a component of the Barents–Kara continental margin. The EB evolved within an entire system of the North Atlantic [55, 66] only after the termination of spreading in the Labrador Sea–Baffin Bay system in the Early Oligocene (C13ny, 33.2 Ma), which divided the Greenland and North American plates.

The western part of the basin exhibits a reliable succession of all referent Cenozoic LMAs beginning from C24no (53.9 Ma), including the present-day 1n [2, 9, 11, 12, 29, 30, 42, 55, 66, 86, 89, 111] (Fig. 1).

The time of the beginning of spreading, however, remains a matter of debate. According to [42], C25no (57.656 Ma) is the earliest LMA. Some researchers believe that opening began at ~58 Ma [2, 88]. If we correlate this age with inversion geomagnetic field scales, it corresponds to C26n, because the period of its formation is 57.7–59.0 [43] or 57.6–57.9 [68] Ma.

The LMA C26n is also considered the beginning of spreading in later work [30]. According to GTS 2020 [74], the age of the formation of C26n is 58.959–59.237 Ma and is slightly younger for the period of the beginning of spreading in the EB. Other researchers suggest the beginning of spreading occurred between C25n?/C24no (57.656–53.9 Ma) [61]. We accept the dominant viewpoint on the beginning of spreading at ~56 Ma [9, 36, 38, 42, 44, 50, 76, 93]. This age is based on the correlation with LMA C25n, which is limited by the age of 57.1–54.0 [43, 73, 98] or 56.4–55.9 [68] Ma depending on the geomagnetic polarity scale. According to GTS 2020 [74], the age of LMA C25n is limited to the period of 57.656–57.1 Ma, i.e., the spreading of the EB began at 57.4 Ma.

The accepted EB geodynamic settings that occurred at ~45 Ma (C21no–C20no, 47.760–43.450 Ma) include the change in the direction of spreading and the transition from slow to ultraslow spreading [2, 66]. These are clearly correlated with the changed rates and directions of spreading in the Norwegian–Greenland Basin [62, 70, 71]. The reconstruction of plate movement in the Northern Hemisphere was global, because this period saw a kinematic reconstruction of the Pacific Ocean plates [16].

The prevailing viewpoint is based on a comprehensive study of the ACEX drill core, whose section contains a long stratigraphic hiatus from 44.4 to 18.2 Ma [36, 38, 60, 76]. Its beginning coincides with the change in parameters of the EB opening, which resulted in the change in direction of drift lines in the area between C21n (47.760 Ma) and C20n (43.450 Ma) (Table 1, lines for calculation of opening poles, Fig. 2, the positions of chrons).

Between C21n and C20n, the seismic record of all profiles contain a reference reflector typical of the EB, which is recognized as a reference in seismostratigraphic works based on the Cenozoic age of the formation of the basin [9, 44, 56, 93].

The first traces of seasonal ice are recorded in the ACEX drill core at ~46 Ma [37], which indicates climate change reflected in a sharp change of seismic reflections above the reflector of ~45 Ma [93]. It is suggested that the climate change is a result of the

Table 1. Indexation of chrons of geomagnetic polarity and opening poles of the North American Plate relative to the Eurasian Plate

Chrons/(subchrons) of geomagnetic polarity, LMA, TLMA			Age, Ma	Momentary opening poles		Opening half-angles, °
indexation, (after [98])	LMA, TLMA (in text)	LMA, TLMA (in figures)		latitude, ° (N)	longitude, ° (E)	
C1no*	C1no	1no	0.773	60.32	140.4	0.0790
C2ny*	C2ny	2ny	1.775	63.65	135.8	0.1815
C2An.1ny*	C2An.1ny	2An.1y	2.595	63.81	138.16	0.2690
C2An.3no*	C2An.3no	2An.3o	3.596	62.94	139.02	0.3720
C3n.1ny*	C3n.1ny	3n.1y	4.187	62.38	137.91	0.4290
C3n.4no*	C3n.4no	3n.4o	5.235	62.1	138.19	0.5380
C3An.1ny*	C3An.1ny	3An.1y	6.033	62.68	135.93	0.6110
C3An.2no*	C3An.2no	3An.2o	6.727	63.59	135.57	0.6965
C4n.1ny*	C4n.1ny	4n.1y	7.537	63.56	137.83	0.787
C4n.2no*	C4n.2no	4n.2o	8.125	64.25	137.09	0.876
C4Ano*	C4Ano	4Ao	9.105	64.64	135.91	1.0085
C5n.1ny*	C5n.1ny	5n.1y	9.786	67.44	134.9	1.1365
C5n.2no*	C5n.2no	5n.2o	11.056	68.18	133.9	1.3065
C5An.2no*	C5An.2no	5An.2o	12.474	67.22	136.07	1.4860
C5ACny*	C5ACy	5ACy	13.739	64.35	136.69	1.6075
C5ADno*	C5ADo	5ADo	14.609	65.98	135.58	1.761
C5Cn.1ny*	C5Cn.1y	5Cn.1y	15.994	68.06	135.87	2.0055
C5Dny*	C5Dy	5Dy	17.154	68.2	134.84	2.1635
C5Eny*	C5Ey	5Ey	18.007	69.05	133.69	2.3115
C6ny*	C6ny	6ny	18.636	70.71	131.3	2.4635
C6no*	C6no	6no	19.535	69.38	132.94	2.5346
C6AA (C6AAny–C6AAr.2n)	C6AA		21.426	–	–	–
C7n (C7n.1ny–C7Ano)	C7n	C7n	24.396	–	–	–
C8n.1n	C8ny	8ny	25.099	–	–	–
C9n (C9ny–C9no)	C9n		26.930	–	–	–
C12ny	C12ny		30.591	–	–	–
C12no	C12no	12no	30.977	–	–	–
C13ny**	C13ny	13ny	33.214	68.22	131.53	3.825
C13no	C13no	13no	33.726	–	–	–
C15ny	C15ny	15ny	35.102	–	–	–
C18n.1n	C18ny	18ny	38.398	–	–	–
C18n.2n	C18no	18no	40.073	67.72	133.91	4.625
C20ny	C20ny	20ny	42.196	–	–	–
C20no	C20no	20no	43.450	–	–	–
C21ny	C21ny	21ny	46.235	–	–	–
C21no**	C21no	21no	47.76	65.38	138.44	5.48
C22ny	C22ny	22ny	48.878	64.52	138.18	5.75
C22no**	C22no	22no	49.666	64.52	138.18	5.75
C23n.1ny	C23ny	23ny	50.767	–	–	–
C23n.2no	C23no	23no	51.724	–	–	–
C24n.1ny	C24ny	24ny	52.540	–	–	–
C24n.3no**	C24no	24no	53.900	63.07	144.26	6.41
C25ny	C25ny	25ny	57.101	–	–	–
C25no	C25no	25no	57.656	–	–	–
C26n (C26ny–C26no)	C26n	–	59.098	–	–	–

Magnetic anomalies: LMA, linear; TLMA, theoretical linear; the age indexation according to geomagnetic field inversion scale after [98]; single chrons or subchrons of direct polarity (normal) are divided into the age of the beginning of its formation (o, old) and/or end (y, young); *, opening poles (1no–6no) after [89]; **, opening poles (13ny–24no) after [66].

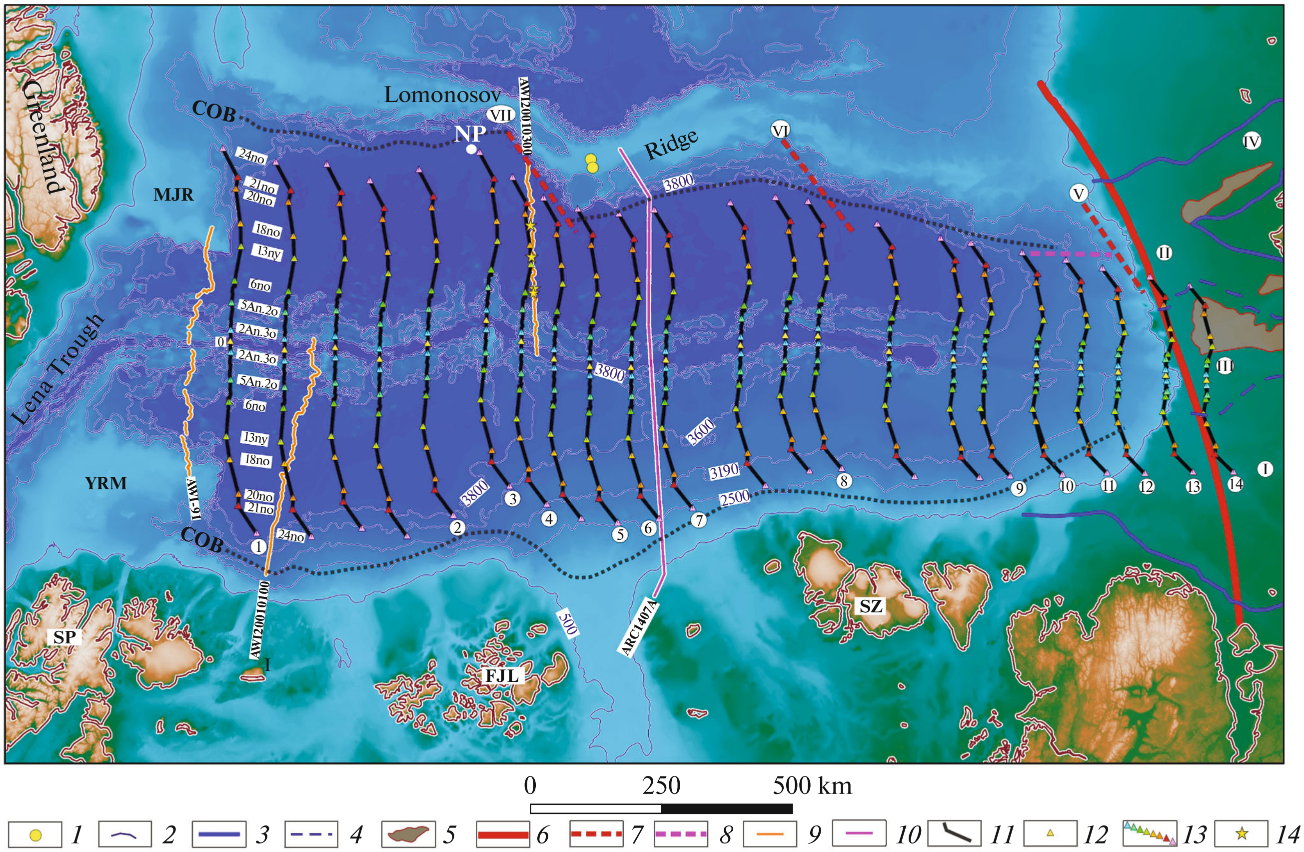

Fig. 6. The positions of drift lines in the Eurasia Basin. Arabian numbers, the numbers of drift lines. COB, continent–ocean boundary; MJR, Morris Jessup Rise; YRM, Yermak Plateau; SP, Spitsbergen Archipelago; FJL, Severnaya Zemlya Archipelago. I–IV, rifting system of the Laptev Sea (1st order structures) after [28, 52]: I, Ust Lena rift-related basin; II, Anzhu rift zone; III, East Laptev province of horsts and grabens; IV, Novosibirsk rift; V–VI, possible Early Cenozoic paleotransform faults in the Amundsen Basin: V, East Lomonosov; VI, Central–East Lomonosov; VII, Central Lomonosov after [49, 92]. (*1*) Position of ACEX drilling boreholes after [38]; (*2*) isobaths of 500, 2500, 3190, 3600, and 3800 m; (*3*, *4*) contours of structures (I–IV) of rift system of the Laptev Sea after [28, 52]: (*3*) rift system; (*4*) 1st order structure; (*5*) main rises; (*6*) possible position of the Khatanga Lomonosov Fault Zone; (*7*, *8*) position of possible structures in the Amundsen Basin (V–VII); (*7*) Early Paleozoic paleotransform faults; (*8*) East Amundsen paleorift; (*9*, *10*) seismic profiles: (*9*) AWI (Germany) after [44, 56, 79, 82]; (*10*) ARC1407A (Russia) after [93]; (*11*) theoretical drift lines; (*12*) position of the center of the rift valley; (*13*) theoretical position of reference chrons (2An.3o–24no); (*14*) points of onlap of key sedimentary sequences on oceanic basement along the line of AWI20010300 seismic profile after [44] (Table 3, Unit-1a, Unit-1b, Unit-1c, Unit-2 for position of points, see Figs. 8, 10).

change in tectonic setting in the Northern Hemisphere [93].

The next key event in the EB was caused by the termination of spreading in the Labrador Sea–Baffin Bay system in the Early Oligocene (C13ny, 33.2 Ma) [97]. It is considered that this age corresponds to the beginning of opening of its westernmost segment between the Yermak Plateau and Morris Jessup Rise [2, 55, 66, 93].

This event has different estimations of its age and scale. If we consider the seismostratigraphic models based on the Cenozoic age of the formation of the EB, the key difference between [93] and other studies [9, 44, 56, 82] is related to the recognition of the reference boundary with the age of ~34 Ma (C13ny, 33.2 [74]).

The presence of this boundary is substantiated by the termination of the Eurekan Orogeny caused by incorporation of the Greenland Plate into the structure of the North American Plate [2, 42, 66, 97]. The Eurekan Orogeny significantly affected only limited areas: the Queen Elisabeth Islands (Canadian Arctic Archipelago), the northern and northeastern margins of Greenland, the western coast and central part of the Spitsbergen Archipelago, the westernmost part of the Lomonosov Ridge, Yermak Plateau, and Morris Jessup Rise [49, 97, 109].

The end of a local, probably, medium-scale event in the Arctic could not trigger a significant stratigraphic reconstruction in the entire EB.

There is also an age uncertainty. The segment between the Yermak Plateau and Morris Jessup Rise is significantly narrower relative to the rest of the EB because of the later opening of this area (Fig. 1). According to various tectonic reconstructions, the separation of the Yermak Plateau from the Morris Jessup Rise occurred earlier in C12ny (30.591 Ma) [42] or synchronously with C13n (33.214–33.72 Ma) [2, 56] or possibly during the period of 35.3–33.7 Ma [30]. In another work [78], the age of the first identified LMA decreases to C9n (26.420–27.439 Ma).

Ambiguous interpretation of these tectonic ideas and sedimentation regimes leads to equivocal interpretation of ACEX deep-water drilling data in the Lomonosov Ridge and for the further key events in the EB.

The period of 18.2–17.5 Ma saw a sharp opening of the Fram Strait (the present-day Lena Trough), which connected the northeastern part of the North Atlantic Basin and EB [36, 37, 76]. In the Arctic Ocean, this led to very fast transition from an oxygen-poor lacustrine phase to an estuary marine phase, which was replaced by an oceanic phase as a result of expansion and deepening of the Fram Strait during the period of 11.56–9.36 Ma. In a geodynamic sense, this means that the age of the phase change was independent from the time of the beginning of opening of the EB between the Morris Jessup Rise and Yermak Plateau, because it occurred significantly earlier than 18.2 Ma according to tectonic reconstructions.

According to an Os isotope study, the stratigraphic hiatus spanned a short period of 34–36 Ma (the Late Eocene), its duration was only 400000 ka, and the opening of the Fram Strait began at ~36 Ma [100] leading to marine circulation. The presence of a short stratigraphic hiatus is supported by many Russian specialists [13, 21, 26].

RECONSTRUCTIONS AND INTERPRETATION

It is evident that the tectonic–stratigraphic evolution of the EB is contradictory from 36–33.2 Ma.

No LMAs of C13n (~33.214–33.726 Ma) are traced between the Morris Jessup Rise and Yermak Plateau [2, 30, 42, 56, 66, 78], i.e., this segment was divided later. The full spreading in this segment at ages less than 33.5–33.2 Ma became ultraslow (1.1–1.5 cm/year) [2, 66]. According to theoretical calculations, the strait width for the formation of the full link between the oceans should be no less than 50 km [76]. At these low spreading rates, the formation of an oceanic crust area of this width requires a period of 3.0–4.5 Ma. Even if we accept the age of ~33.5 Ma (the middle of C13n, 33.214–33.726 Ma) as the beginning of rifting extension between the Morris Jessup Rise and Yermak Plateau, a strait of the necessary width for a proper water exchange could theoretically form no earlier than 30.5–29.0 Ma.

The main principle difference in the LMA interpretation in the western part of the EB is related to the identification of the oldest magnetic anomaly, which began to form in a fragmentary way between the Morris Jessup Rise and Yermak Plateau (Fig. 1). This LMA is confined to the range of C12no–8ny (30.977–25.987 Ma) [42] in contrast to C7n (24.025–24.459 Ma) according to [55]. This difference leads to uncertain results of seismostratigraphic positioning.

The results of the LMA interpretation [42] were the basis for the interpretation of seismic data in the western part of the Amundsen Basin [44]. The interpretation of seismic data in the western part of the Nansen Basin [56] was based on the results of the LMA interpretation [55]. The LMA in the western part of the Nansen Basin was re-identified during the correlation of the nearest Russian (Fig. 1, profiles ARC1103, ARC1104, ARC1105, and ARC1106) and Norwegian seismic profiles [9].

The work [42] described warranted identification of the beginning of this LMA by 8ny (25.987 Ma). A positive maximum of the magnetic anomaly, which was identified by C9n (26.420–27.439 Ma) [42], was identified in [78].

The determination of the precise time of the beginning of opening of the Fram Strait is still under discussion due to the complex geodynamic setting and limited geological–geophysical data. The idea that the earliest LMA of C6no (~19.6 Ma) appears fragmentarily only in the northernmost part of the Lena Trough connected with the EB is prevailing [55]. The first continuous LMA in the segment of the Lena Trough and the southward Molloy Basin is C5n (~10.4 Ma) and a continuous oceanic corridor formed in the Early Miocene (20–15 Ma). The earliest identified chron for this segment is C6AA (~21 Ma) [53].

The considered age interval of the beginning of the formation of the Lena Trough corresponds to the ACEX stratigraphic model, in which the age of the termination of the long stratigraphic hiatus is accepted as ~18.2 Ma [36, 37, 76] and absolutely contradicts an alternative model, in which the age of the termination of the short hiatus is ~34 Ma [13, 21, 26, 100].

In our interpretation, we accepted the classical ACEX model [36, 38, 76].

Various tectonic reconstructions are presented for the junction area of the oceanic EB and the continental crust of the Laptev Sea: the displacement of the Gakkel and Lomonosov ridges from the rift system of the Laptev Sea shelf along the transform Khatanga–Lomonosov Zone [51]; the motion of the Lomonosov Ridge in the structure of the North American Plate without the formation of a strike-slip fault system [5, 19]; and the transform movement of the Lomonosov Ridge relative to the Eurasia margin along the Khatanga–Lomonosov Fault Zone only in the initial spreading stage of the EB evolution in the Early Cenozoic until the second half of the Eocene and the termination of the transform movement due to the change in the direction of plate movement in the Northern Hemisphere [16, 28, 93].

During the correlation between the reference seismic reflectors and the LMAs, it is important which segment of the system is interpreted: a geodynamically calm area or an area of insignificant transform movements related to local jumps of the spreading axis. The ARC1407A seismic profile is located approximately in the center of the EB.

In spite of the significant distance of the ARC1407A seismic profile from the Laptev Sea, there is a high probability of discovery of local transform movements in the central and eastern parts of the EB, because the spreading rate decreases and instability increases toward the continental margin of the Laptev Sea, which is related to the approach to spreading poles. The junction area of tectonic structures plays an important role in the identification of the temporal intervals of local jumps of the spreading axis.

The aeromagnetic data used in the LMA identification in the eastern part of the EB are unreliable due to their large errors leading to the search for an alternative verification of local jumps of the spreading axis. The standard solution is the comparison of the position of the drift lines with geomorphological and tectonic elements. This analysis for the EB and its eastern part has previously been conducted [2, 63, 93], but we expanded the area of the analysis.

Analysis of Drift Lines and Migration of Momentary Rotation Poles

Drift lines can be calculated on the basis of the position of momentary opening poles. In the case of the necessary tracing of the peculiarities of the opening from the present-day spreading center toward the deep-water basins, the calculations are conducted using half angles, which means symmetrical spreading. In the case of asymmetric spreading, this assumption, on one hand, leads to some distortions, but, on the other hand, there are areas of jumps of the spreading axis within single ridge segments.

The results of the recent calculations of the positions of opening poles [2, 66, 89] coincide, therefore the estimations of the rate and direction of opening of the EB [2, 66] also coincide. Thus, we used the results of the analysis of peculiarities of spreading for the westernmost sector of the eastern part of the EB [2], which showed the following: the period of C24no–C20no (53.9–43.45 Ma) had the maximum asymmetry, indicating frequent jumps of the spreading axis within single segments; asymmetry was strongly reduced in the period of C20no–13n (~43.45–33.5 Ma) leading to segmentation along the spreading paleoaxis, when the areas of good coincidence of the present-day and ancient spreading axis (LMA) are replaced by an area of inconsistency, indicating local jumps of spreading axis; almost full symmetry is observed during at the period of C6no–2nA (~19.6–3.6 Ma). These principles are clearly confirmed by the position of the drift lines (Fig. 6).

The sedimentary cover of the Nansen Basin is significantly thicker than that of the Amundsen Basin [79, 93]; thus the continental slope area of the margin of the Kara Sea is strongly smoothed. Therefore, the distances from the end of the drift lines (C24no (53.9 Ma)) to topographic isolines of the Lomonosov Ridge from the Amundsen Basin were compared during visual estimation, which is based on seafloor topography.

Use of a continent–ocean boundary is an analogous solution for visual comparison. Due to the scarce deep seismic exploration data, we used gravity field anomalies. This determination of the continent–ocean boundary, especially in areas of smoothed topography of continental margins, is rather conditional. The position of this boundary corresponds to the maximum gradients of Bouguer anomalies [2, 50, 55], but, because of the highly ambiguous position of the gradient in the eastern part of the EB, we supplemented the commonly accepted standard with (i) additional use of WGM-2012 isostatic anomalies calculated in the Airy–Heiskanen model [41] and (ii) directed determination of the maximum horizontal gradients within relatively straight areas of the Barents–Kara continental margin and Lomonosov Ridge.

The comparison of the directions of drift lines, the seafloor topography, and the position of the continent–ocean boundary indicates that during the Early Cenozoic the EB evolved within individual segments (between drift lines 1–3, 3–5, 5–8, 8–10, 10–12, and 12–13), which were inherited from the tectonic structure of the continental margin [27, 92, 93] (Fig. 6). The segments were divided by transform faults with insignificant displacement. The first segment contains a subsegment (Fig. 6) between drift lines 1–2.

The suggested Early Cenozoic paleotransform fault [61, 92, 102] (we call it the Central Lomonosov fault) clearly occurs in the direction of drift lines 4–5 in the period of C24no (53.9 Ma)–C21no (47.760 Ma) (Fig. 6). The curve in the center of the eastern part of the Lomonosov Ridge, which is located exactly on a traverse of drift line 8, indicates the presence of one more paleotransform fault with the possible name of the Central–East Lomonosov fault (Fig. 6). The paleotransforms in the Amundsen Basin should be mirrored in the Nansen Basin, but the absence of reliable geophysical data prevent their identification, whereas the morphological criteria (as in the Lomonosov Ridge) do not work because of the thick sedimentary cover.

Drift line 14 on the shelf on the Gakkel Ridge continuation shows that the rift system of the Laptev Sea is approximately two times wider, indicating intense Upper Cretaceous (?) extension, which has already been emphasized many times [51] (Fig. 6).

Drift lines 13–14 show that the direction of the Khatanga–Lomonosov Fault Zone [28] coincides with drift lines only for C20no (43.450 Ma)–C13ny (33.214 Ma) and strongly differs for other Cenozoic periods, reflecting the complex and multistage evolution of the formation of the easternmost area of the EB (Figs. 6, 7).

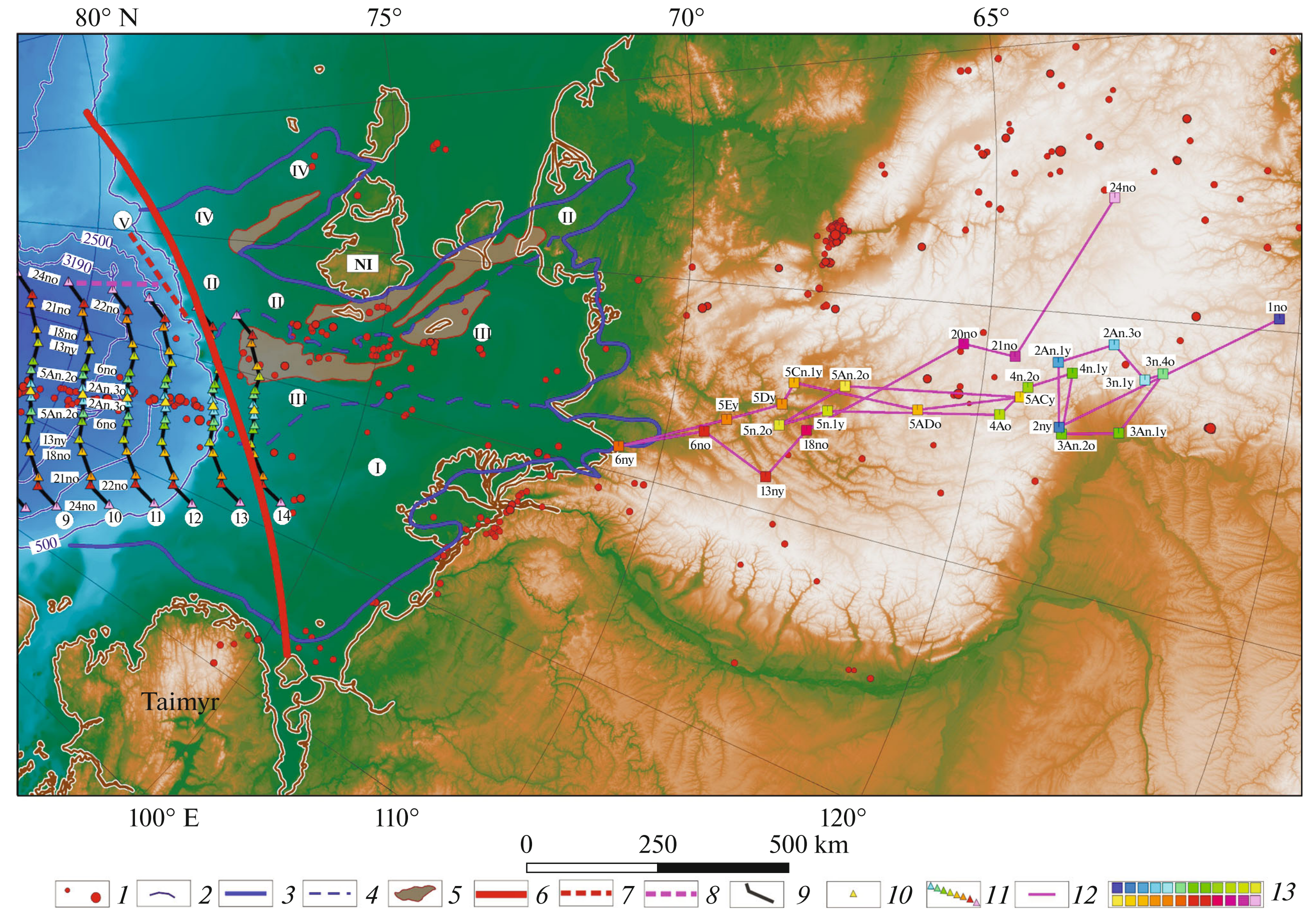

Fig. 7. The position of momentary opening poles for the Eurasian and North American plates after [66, 89] (IBCAO v. 4 bathymetric model [77]). NI, Novosibirsk Island; I–IV, rift-related system of the Laptev Sea after [28, 52]: I, Ust Lena rift-related basin; II, Anzhu rift zone; III, East Laptev province of horsts and grabens; IV, Novosibirsk rift; V, East Lomonosov. (*1*) Earthquakes in a range of 3.3 – 6.9 *M* (intensity is proportional to sizes) after [10]; (*2*) isobaths of 500, 2500, 3190, 3600, and 3800 m; (*3*, *4*) contours of structures (I–IV) of rift-related structure of the Laptev Sea after [28, 52]: (*3*) rift system; (*4*) 1st order structures; (*5*) main rises; (*6*) possible position of the Khatanga–Lomonosov Fault Zone; (*7*, *8*) position of possible Early Cenozoic paleotransform fault (V) in the Amundsen Basin; (*8*) East Amundsen paleorift; (*9*) drift line; (*10*) center of the rift valley; (*11*) theoretical position of reference chrons (2An.3o–24no); (*12*) curve of migration of momentary opening poles (1no-6no [89]) and (13ny-24no [66]); (*13*) position of momentary opening poles.

The previously found asymmetry of the distances of the Amundsen and Nansen basins is confirmed beginning from drift line 10 toward the continental margin of the Laptev Sea and is explained by spreading asymmetry during the period of 49–33 Ma [63] (Figs. 6, 7). This asymmetry is most clear in drift line 12, on which C24no (53.9 Ma) is theoretically already located on the Laptev Sea shelf rather in the Nansen Basin, whereas it is located in the Amundsen Basin on the opposite side (Fig. 6).

This asymmetry can be explained by the opening of the EB in this area in the Early Cenozoic in the southeastern part of the Amundsen Basin in front of the Anzhu–Novosibirsk rift system and a further jump of the spreading axis approximately during the period of C21no (47.760 Ma)–C20no (43.450 Ma). This age corresponds to the reconstruction of spreading in the EB and Norwegian–Greenland Basin [66, 71]. In this case, the southeastern part of the Amundsen Basin should host a local paleorift (we name it East Amundsen), whereas the junction with the continental margin should occur along the fault, which we name the East Laptev Paleotransform Fault (Figs. 6, 8).

The period of C20no (43.450 Ma)–C13ny (33.214 Ma) registers the consistent directions of drift lines of the suggested Khatanga–Lomonosov Fault Zone. Very slow rifting with possible simultaneous insignificant displacement (or displacements) along this direction occurred in the easternmost segment of the EB between drift lines 12–13 (Fig. 6).

The kinematic reconstruction of the opening of the Eurasia and North America plates beginning from the period of the formation of C13ny (33.214 Ma) is reflected in the position of the opening poles (Fig. 7).

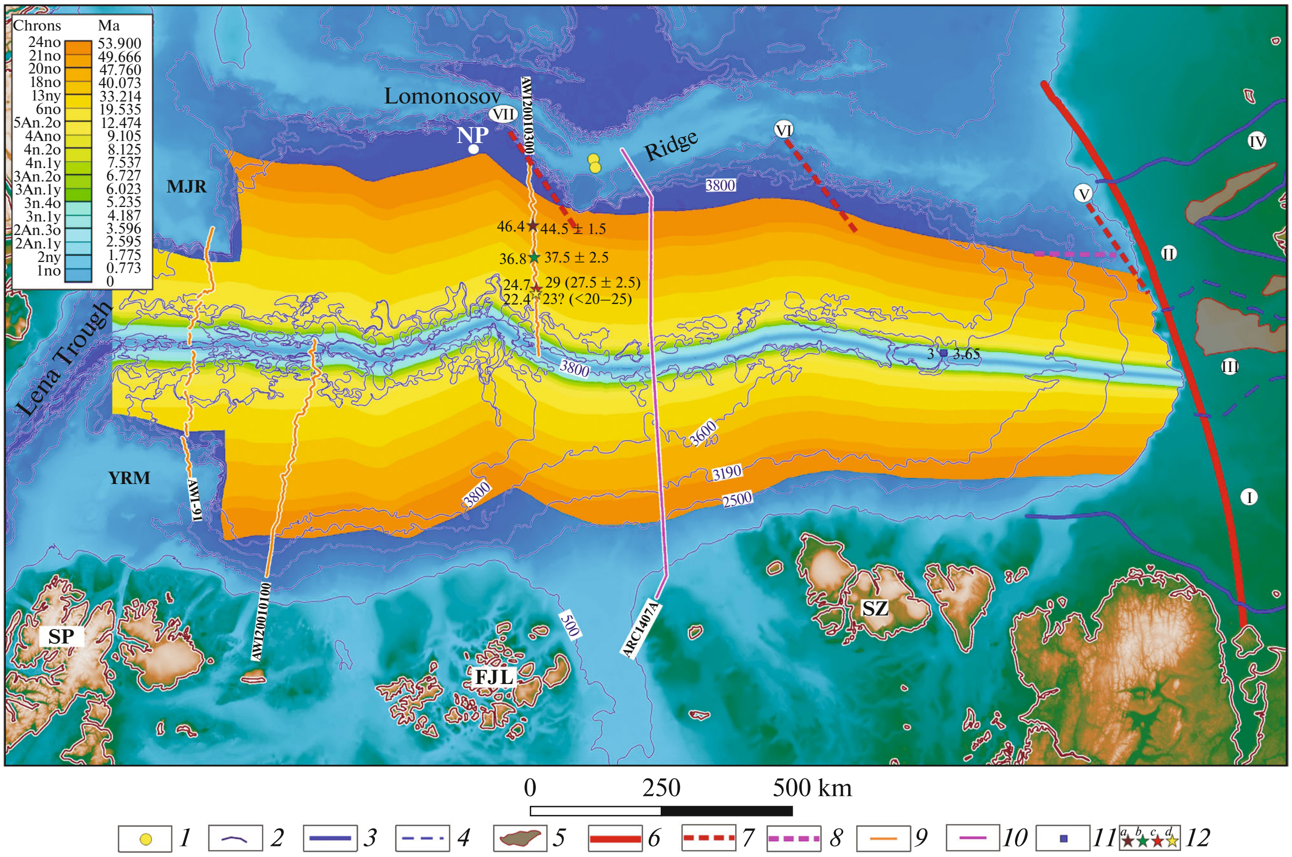

Fig. 8. The theoretical age of the formation of oceanic crust of the Eurasia Basin. NP, North Pole; MJR, Morris Jessup Rise; YRM, Yermak Plateau; SP, Spitsbergen Archipelago; FJL, Franz Josef Land; SZ, Severnaya Zemlya Archipelago. I–IV, rift-related system of the Laptev Sea after [28, 52]. I, Ust'Lena rift-related basin; II, Anzhu rift zone; III, East Laptev province of horsts and grabens; IV, Novosibirsk rift; V–VII, possible Early Cenozoic paleotransform faults in the Amundsen Basin; V, East Lomonosov; VI, Central–East Lomonosov; VII, Central Lomonosov after [49, 92]. (*1*) Position of ACEX drilling boreholes after [38]; (*2*) isobaths of 500, 2500, 3190, 3600, and 3800 m; (*3*, *4*) contours of rift-related system of the Laptev Sea after [28, 52]; (*3*) rift system; (*4*) 1st order structures (I–IV); (*5*) main rises; (*6*) possible position of the Khatanga–Lomonosov Fault Zone; (*7*, *8*) position of possible structures in the Amundsen Basin; (*7*) Early Cenozoic paleotransform faults in the Amundsen Basin (V–VII); (*8*) East Amundsen paleorift; (*9*, *10*) reference seismic profiles: (*9*) AWI (Germany) after [44, 56, 79, 82]; (*10*) ARC1407A (Russia) [93]; (*11*) dredging area of young basalts (the age (Ma) according to the results of geochronological studies after [80] is shown to the right; the theoretical age (Ma) is shown to the left); (*12*) onlap of sedimentary sequences (Table 3, Figs. 6, 10) on oceanic basement along the line of seismic profile AWI20010300 after [44]. The age and determination error (Ma) after [44] is indicated to the right. The theoretical age (Ma) is indicated to the left: *a*, Unit-1a; *b*, Unit-1b; *c*, Unit-1c; *d*, Unit-1c.

It is likely that local jumps of the spreading axis occurred regularly in the easternmost part of the EB, but they are not reflected in geophysical data due to ultraslow rates.

A strong change occurs in C6ny (18.636 Ma), which coincides with the age of the termination of the long stratigraphic hiatus revealed in the ACEX borehole (~18.2 Ma) [36, 37] and the beginning of segmented spreading in the Lena Trough (~19.6 Ma) [55]. Until that time, the displacement of the opening poles generally followed the northwestern direction and changed its direction to the south after that period (Fig. 7).

The change in the direction of the opening poles at ~18.6 Ma led to a change in the opening mechanism in the easternmost part of the EB and the beginning of relatively fast rifting of the continental margin at ultraslow spreading rates starting approximately from 77.8° N.

The instability of the system and a reverse trend to the northern direction during the period of C5ACy–C5n2o (13.739–11.056 Ma) are very important. It can be suggested that the opening in the easternmost segment of the system beginning approximately from 77.5° N (the center of drift line 13–the local curve of isobath of 500 m) began no earlier than C5ACy (13.739 Ma). The section of the ACEX borehole contains a stratigraphic hiatus of 11.6–9.4 Ma, which supports the correlation of events [36, 37].

The almost complete absence of asymmetry for the EB area [2] that hosts the ARC1407A seismic profile is supported by drift lines 6 and 7 (Fig. 6). The near-rift seamounts are clearly limited by C6no (19.6 Ma). There are insignificant differences in distances between C24no (19.6 Ma) and the continent–ocean boundary for drift line 7. The difference in distances for drift line 6 is significantly higher. This indicates that no significant axis jumps occurred at the initial stage of opening in the area of the slope of the Lomonosov Ridge, where the seismic profile is located. The area of the continental slope in the Amundsen Basin was characterized by axis jumps, but its seismic record contains no basement due to the significant thickness of the sedimentary cover [93], thus it is impossible to make a seismostratigraphic positioning for the lowest horizons.

If we rely on the estimations of asymmetry from [2], the EB area with the seismic profile can be divided into the following areas in the first approximation: the central part formed during the period of 19.6–0 Ma (6no) with a high degree of symmetry not exceeding the deviation of 3–5% and the flank formed during the period of 56–19.6 Ma (24no–6no), where asymmetry can reach 5–7% for the most ancient ages in the Amundsen Basin.

Profile ARC1407A lies in a seismotectonically and geodynamically calm segment without significant jumps. These estimations of possible asymmetry are true for the calculations of the theoretical age of the oceanic crust.

Seismostratigraphic Positioning

If we accept the continuous Cenozoic spreading formation of the EB, the classic seismostratigraphic indexation (as in [9, 44, 56, 79, 93]) suggests the identification of the onlap areas (closest to the rift valley) of sedimentary sequences on the oceanic basement, the ages of which are determined from the results of LMA axis identification, which corresponds to the principle of the impossibility of the formation of an older sedimentary sequence than the age of the underlying oceanic crust (Fig. 9).

This method of seismostratigraphic indexation is widespread for the age determination of sediments formed in spreading basins, but it can yield significant errors in this area. This is related to an extremely low navigation precision of aeromagnetic data in this EB area, the error of which can reach tens of kilometers. This is supported by the results of LMA identification along the line of the ARC1407A seismic profile [93] (Fig. 9).

There is the extensive spreading asymmetry, which results in strongly different lengths of the oceanic crust areas formed for the same period in the Amundsen and Nansen basins (Fig. 9).

An alternative solution is related to the determination of the theoretical TLMA position relative to the present-day spreading center using the rotation poles and half angles of opening of the Eurasia and North American plates and the construction of the model of theoretical age of the oceanic crust. The TLMA determination was based on the calculations of the position of drift line with a step of 2.5–5.0 km, thus the given determination errors are valid.

The present-day divergent boundary is accepted as an initial point using the half angles as is done in this work. The spreading axis in regional studies is typically distinguished by the axis of the minimum of free air gravity anomalies above the rift valley. We gave the priority to the IBCAO v4 bathymetry [77], which is based on the MSE data for the Gakkel Ridge (except for the easternmost area), because the compilations of gravity anomalies for the Arctic are smoothed. In areas of minor nontransform displacements of the rift valley and the easternmost part of the EB, we preferred the free air gravity anomalies from the WGM-2012 project [41].

The plate rotation poles, angles, and half angles of spreading used in this work are shown in Table 1. A cycle of glaciomarine sedimentation began ~2.7 Ma that is reliably identified for the western and northwestern margins of the Barents Sea and adjacent deep-water basins by drilling and numerous seismic data [31]. The theoretical TLMA position for this age was calculated by linear interpolation between the nearest C2An.1ny (2.595 Ma) and C2An.3no (3.596 Ma) with known rotation poles [89].

For profile ARC1407A, the local rise in the center of the rift valley, which can be related to neovolcanism judging from the seismic record, is accepted as the position of the present-day spreading center, for which calculations have been made. The present-day volcanic axial ridges and volcanoes are mapped and confirmed by sampling [101] in a closely located area of the rift valley of 85° N of the Gakkel Ridge [90, 101].

The results of TLMA calculations are used in seismostratigraphic interpretation of profile ARC1407A. For some slopes of the near-rift seamounts adjacent to the rift valley of the Gakkel Ridge from the Amundsen Basin, no sedimentary cover was revealed in the junction area of seismic profiles ARC1420 and ARC026 [93] (Fig. 6).

The $^{40}Ar/^{39}Ar$ age of dredged basalts in this area is 3.65 ± 0.01 Ma [80]. To compare the correctness of TLMA calculations, whose age was assigned according to the GTS-2020 [74], we calculated the matrix of the theoretical seafloor age (Fig. 8).

Because of the instability of spreading for the period of the formation of C6ny–5n.1y (18.636–9.786 Ma), which is evident from the sharp displacement of plate rotation poles located closely to the EB, only the TLMA of C5An.2o (12.474 Ma) was used for the calculation of the age matrix in a range of C5 (Fig. 6). Because the geodynamic evolution of the EB area, which is conjugated with the continental margin of the Laptev Sea, remains debatable, the age matrix is cut by an isobath of 500 m (Fig. 8).

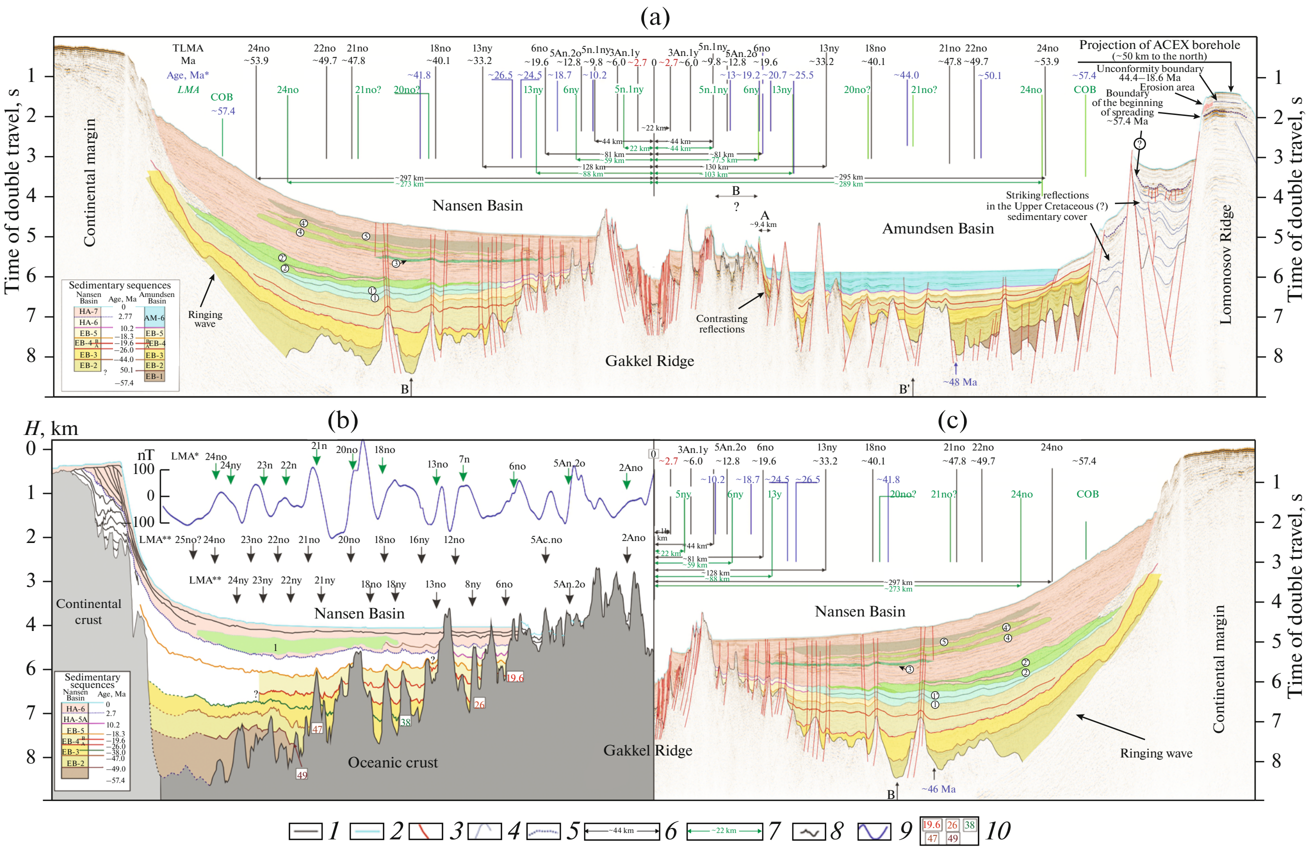

Fig. 9. Seismostratigraphic correlation of seismic profiles ARC1407A and AWI20010100, modified after [18, 56, 93]. a, time section along the ARC1407A seismic profile; b, deep section along seismic profile AWI20010100; c, mirrored image of section of part of ARC1407A seismic profile in the Nansen Basin. TLMA, position of theoretical axes of linear magnetic anomalies and their age (Ma) according to inversion geomagnetic field scale after [98]; LMA, position of axes of linear magnetic anomalies after [93]; LMA*, axes of linear magnetic anomalies and their indexation after [56]; LMA**, axes of linear magnetic anomalies identified after [9]; COB, continent–ocean basin after [93] and the age of the formation according to the inversion geomagnetic field scale after [98]; A, area of fast uplift of the paleowall of the rift valley; B, B', symmetric near-rift depressions in the Nansen and Amundsen basins relatively to the center of the rift valley of the Gakkel Ridge with an insignificant displacement (~2 Ma) of theoretical age of the formation of oceanic crust; C, area of uncertainty of tracing of seismic horizons in the Amundsen Basin; 1, 1'; 2, 2'; 3; 4, 4', and 5, areas with significant or partial loss of correlation of seismic signal interpreted as submarine landslides and turbidite flows. The age (Ma), the theoretical age of oceanic basement in areas of onlap of identified sedimentary sequences. The points with the age of 2.7 Ma (red) are determined by linear interpolation between nearest TLMAs (Table 1). (*1*) Basement topography; (*2*) seafloor surface above sedimentary cover; (*3*) faults; (*4*) boundaries in sedimentary cover of the Lomonosov Ridge; (*5*) possible position of the boundary in sedimentary cover on the Lomonosov Ridge corresponding to the beginning of spreading in the Eurasia Basin; (*6*, *7*) distance from the center of the rift axis to theoretical axes of LMAs (*6*) and LMA axes (*7*) after [93]; (*8*) surface of the oceanic basement; (*9*) MAF curve; (*10*) age of oceanic crust in areas of onlap of sedimentary sequences (Ma).

The starting and final points of the dredge profile were further extracted from the matrix. The theoretical ages for the starting (81°12.76′ N, 121°25.87′ E) and final (81°12.15′ N, 121°31.26′ E) points of the profile are 2.8 and 3.2 Ma, respectively, indicating the consistency of theoretical calculations and laboratory determinations.

Seismic profile AWI20010300, which is located ~120 km from the ARC1407A seismic profile [44], was used as a reference in the western part of the Amundsen Basin. Due to the absence of transverse profiles connecting the two profiles, the correctness of visual comparison of seismic sequences is in doubt.

To control this, the values for onlap points of sedimentary layers on the oceanic basement along seismic profile AWI20010300 [44] were extracted from the theoretical age matrix. The results of the comparison show very close ages confined to the LMA [44] and those that were theoretically determined (Table 2).

The difference in age determination for the top of sequence Unit-1a (44.5 Ma) [73], 44.8 Ma [98]) of ~1.6 Ma almost falls in the determination error of ±1.5 Ma [44]. The age of 44.8 Ma corresponds to the reconstruction of movements of plates, thus this age difference can reflect the duration of the reconstruction.

The age difference of the top of sequence Unit-1c (27.5 Ma [73] or 28 Ma [97]) of ~3.3 Ma slightly

Table 2. Comparison of the age of the top of sedimentary sequences along the line of seismic profile AWI20010300 with results of determination of theoretical age extracted from value matrix (Fig. 8)

Sedimentary sequence[1]	Age of the top after scale of 2012,[2] Ma	Determination error,[3] Ma	Used LMA*,[4]	LMA age after scale of 2012,[5] Ma	LMA age after scale of 2020,[6] Ma	LMA age after scale of 2020,[7] Ma	Theoretic age of the top after scale of 2020,[8] Ma	Difference in determination of ages after scale of 2020,[9] Ma
Unit 1a	44.5	±1.5	C21ny–20no	45.724–42.301	46.235–43.450	44.8	46.4	1.6
Unit 1b	37.5	±2.5	C18o–15y	39.698–33.705	40.073–35.102	37.6	36.8	0.8
Unit 1c	27.5	±2.5	C12o–C8y	24.984–30.591	30.977–25.099	28	24.7	3.3
Unit 2	23(?)	< 25–20	<C8y	24.984	25.099	23	22.4	–0.6

[1], indexation of sedimentary sequences after [44]; [2], the age of the top of sedimentary sequences according to geomagnetic field inversion scale after [44, 73]; [3], determination error of the age of the top of sedimentary sequences after [44]; [4], Used LMA for the determination of the age of the top of sedimentary sequences after [42, 44]; [5], [6], the age range of LMA intervals according to geomagnetic field inversion scale: [5], after [73]; [6], after [98]; [7], the age of the top of sedimentary sequences according to geomagnetic field inversion scale after [98]; [8], theoretical age of the oceanic crust at the onlap area of the top of sedimentary sequence according to geomagnetic field inversion scale after [98]; [9], the Difference in determination of ages of the top of sedimentary sequences determined after LMAs and the theoretical age of the oceanic crust (according to geomagnetic field inversion scale after [98]).

exceeds the determination error of ±2.5 Ma [44]. It is noted that the onlap point of the sedimentary sequence on the oceanic basement is located within the near-rift seamounts in the area of a sharp increase in the basement, thus the age of this sequence could be younger [44].

Seismic profile AWI20010100, which is significantly remote from the ARC1407A seismic profile [56], was used as a reference in the western part of the Nansen Basin (Figs. 1, 6). The additional reference horizons, whose ages were not analyzed, were traced in stratigraphycally-related sequences (Fig. 9b). Not changing the positions of the reference horizons, we correlated them with the LMAs using the results of LMA re-identification [9], which were specially conducted to correlate the results of Norwegian studies with the nearest Russian seismic profiles.

INTERPRETATION OF SEISMIC PROFILE ARC1407A

Comparison of the TMLAs and LMAs along the ARC1407A Seismic Profile Line

The visual analysis of the TMLA positions and results of identified LMAs from [93] shows the consistent and absolutely different positions in the Amundsen and Nansen basins, respectively (Fig. 9a). The results of the comparison of reliably identified LMAs and TLMAs as qualitative estimations are shown in Table 3.

The positions of the TLMAs and LMAs in the Amundsen Basin for C5n.1ny, C6ny, and C24no coincide because of the sufficient density of aeromagnetic data in this area (Fig. 4). For the Amundsen Basin, a single significant difference was revealed for C13ny (~33.2 Ma). A single TMLA and LMA coincidence for the Nansen Basin within the chosen errors (<7%) is observed in the C24no area. The age error for the LMA of C5n.1ny, C6ny, and C13ny varies from 25 to 100%, which cannot be explained by extensive jumps of the spreading axis, because their signatures are not visible from seismic data (Fig. 9a).

The extensive asymmetry of opening for the LMA of C5n.1ny is noteworthy, because the length of the oceanic crust area formed for the same period of time in the Amundsen Basin is two times wider than that in the Nansen Basin.

The LMA of C5n.1ny falls in a period that began from the Early Miocene (C6no, 19.535 Ma), when the EB formed as a single system with North Atlantic. The works [2, 66, 89] dedicated to the LMA identification in the North Atlantic and EB show a high spreading symmetry in this period of the evolution of the system, which excludes possible double asymmetry.

This asymmetry can be geodynamically explained only by a long jump of the spreading axis, but this should have led to the formation of a paleorift valley in the Amundsen Basin, which is absent in the seismic data, and transform faults should be present, which are not visible from remote data (bathymetry, gravimetry, and magnetometry).

Judging from these data, all LMAs identified in the Nansen Basin and LMAs of 13ny (33.214 Ma) in the Amundsen Basin have imprecise positions.

Table 3. Calculations of disproportions of the LMA position and age after [93] in the Amundsen and Nansen basins along the line of ARC1407A seismic profile relative to the rift axis of the Gakkel Ridge (Fig. 9a)

LMA	Amundsen Basin					Nansen Basin				Comparison of difference in LMA distances from the spreading center in basins***	
	age, Ma*	distance, km**	theoretic age, Ma	age difference, Ma	distance proportion, %	distance, km**	theoretic age, Ma	age difference, Ma	distance proportion, %	distance proportion, km	distance proportion, %
5n.1ny	~9.8	44	9.8	0	0	22	4.8	5	100	22	100
6ny	~18.6	77.5	19.2	0.6	3	59	13.9	4.7	25	18.5	31
13ny	~33.2	103	25.2	8	24	88	21.2	12	36	15	17
24no	~53.9	289	53.5	0.4	0.7	273	52.3	1.6	3	16	6

The age indexation is according to geomagnetic field inversion scale after [98]; single chrons or subchrons of direct polarity (normal) are divided into the age of the beginning of its formation (o, old) or/and end (y—young); *, the age of chron according to geomagnetic field inversion scale after [98]; **, distance along the profile line from the spreading center to LMAs; ***, proportion of distances along the profile line from the spreading center to the position of LMAs in the Amundsen and Nansen basins.

Age Correlation of the Reference Reflectors and Sedimentary Sequences Recognized on Seismic Profile ARC1407A

The age indexation of reflectors, which are distinguished in the lower and middle part of the section of the sedimentary cover, was conducted using traditional correlation of areas adjacent to the oceanic basement, whose ages were determined by TMLA position (Figs. 9a, 9b).

The reflector of the ARC1407 seismic profile area above the Lomonosov Ridge was indexed according to the ACEX drilling results by double projection of profile AWI 91090 on profile ARC1407 through the intermediate AWI 91091 profile [22]. Because this area of the Lomonosov Ridge is flat and seismic data in the projection area show no faults in the upper part of the sedimentary section, a similar approach from a geographical viewpoint is correct for tracing the most contrasting and typical reflectors (Fig. 9a). There are only two striking reflectors: the boundary of the Middle Cenozoic unconformity of 44.4–18.6 Ma and the boundary that registers the beginning of spreading in the EB at ~57.4 Ma [98] according to the stratigraphic position [36, 37].

If we consider the seismic profile toward the Amundsen Basin, there is an erosion area, which cuts the boundary of the Middle Cenozoic unconformity, toward the slope of the Lomonosov Ridge in the upper part of the section (Fig. 9a). The same pattern is observed for profile AWI 91090 [81], thus it is impossible to make a correct tracing of this reflector to the graben after the slope even using paleosmoothing of the reflector. This is also true for the boundary that registers the beginning of spreading in the EB, because it is not traced on the slope.

The visual comparison of the seismic section of the uplifted part of the Lomonosov Ridge and a deep graben and a slope, which occur toward the Amundsen Basin, remains possible. One possible boundary of the beginning of spreading of ~57.4 Ma is a single reflector with a typical contrasting feature. With some assumptions, it can be traced in the graben and the next upper slope area, but it is divided from the lower slope area by a series of faults with a chaotic seismic record between (Fig. 9a). Thus, during the interpretation of the EB seismic data, we generally compared the results with the ACEX borehole section.

Sedimentary Sequence EB-1

Because of the thick sedimentary cover within the continental slopes and adjacent deep-water Nansen Basin, the tracing of the lowermost reflector interpreted as the basement is impossible, because it falls in the zone of multiple reflections. The Nansen Basin thus has a problem of identification and age indexation of the lowermost reflector in the sedimentary cover, which is indexed at ~50 Ma [93]. The age indexation of this reflector was calculated for seismic profiles, which are located in front of the FJLA continental margin [93] according to the results of LMA identification in the area, which has been sufficiently studied by aeromagnetic surveys.

This reflector in seismic profile ARC1407A is clearly observed in the Amundsen Basin and, according to theoretical calculations, has an age of ~50.1 Ma (Fig. 9a). This reflector is traced in the western part of the Nansen Basin on seismic profile AWI20010100

(Fig. 6, drift line 8) and its age is estimated at 49 Ma (Fig. 9b). These age values are similar to the maximum Cenozoic sea level point (Fig. 10).

Correlating with ACEX drilling results, this age corresponds to a geological boundary of ~49.7 Ma, which is characterized by the oldest preserved biosiliceous taxon of 50.1 Ma, the beginning of onset of biosiliceous silt of 49.7 Ma, and episodic fresh-water conditions of 48.6–49.2 Ma [36] that explain the formation of contrasting and typical reflections in the seismic record (Fig. 9a).

Sedimentary Sequence EB-2

The above located reflector is a reference clearly observed in all available EB seismic profiles (Figs. 9a, 9b). It divides a rhythmic sequence with contrasting reflections (EB-2) from a sequence with much lower contrasting reflections (EB-3). The age indexations of this reflector, which was conducted by different researchers for seismic profiles located in different EB regions, are close to each other [44, 56, 93].

In the western part of the Nansen Basin, the age of this reflector is identified with the top of the sedimentary sequence NB-1A with the age of 48 Ma [55] (Fig. 10). Our connection of this reflecting horizon to the LMA shows the similar result 47 Ma (Fig. 9b). In the eastern part of the western sector of the Amundsen Basin, this reflector is indexed at 44.5 Ma [44]. In work [93] based on a significant volume of domestic seismic data, this reflector is indexed at 45 Ma and is traditionally correlated with the beginning of a stratigraphic unconformity (45.4 Ma), which is based on drilling results in the Lomonosov Ridge [36, 37]. For this reflector of the ARC1407A seismic profile in the Amundsen and Nansen basins, we calculated the ages of ~44 and 41.8 Ma, respectively.

Sedimentary Sequence EB-3

The onlap of the above located characteristic sedimentary sequence EB-3 on the oceanic basement shows high symmetry in the Nansen (~26.5 Ma) and Amundsen (~25.5 Ma) basins (Figs. 9a, 9c). This reflector is clearly observed in the western part of the Nansen Basin in seismic profile AWI20010100 [55] (Figs. 9b, 10). The age indexation of this reflector is similar (26 Ma) (Fig. 9b). In the Amundsen Basin, the top of sequence EB-3 corresponds to the top of layer Unit-1c of ~27.5 ± 2.5 Ma [44] (Fig. 10).

Similar interpretation results for the boundary of ~26 Ma contradict the results of [93, 94], in which the reflector slightly located above is recognized as one of the reference reflectors for the Arctic Basin with the age of 34 Ma (~33.2 Ma [74]). If we accept the seismostratigraphic model of [93], the age of the EB-3 top should thus be older than 34 Ma, i.e., the difference with results of our interpretation reaches ~10 Ma leaving ~17% of the total age of the EB existence (a beginning of ~57.4 Ma).

If we use the mathematic estimations of the precision of coincident identification of the LMA 13ny [93], the difference in distances from its positions in the Amundsen and Nansen basins to the present-day spreading center is ~15 km or ~17% (Table 3, Fig. 9a).

The period of the formation of C13n was characterized by extremely low spreading rates, which are lower than the present-day ones [2]. The seismic data show that the width of the present-day rift valley is ~22 km, whereas the theoretical calculations show that it formed over the last ~2.7 Ma (Figs. 8, 9a). The asymmetry of the LMA positions in 15 km should thus lead to the formation of the paleorift valley in the Amundsen Basin, which is invisible from seismic data. More disproportion is observed in comparison of the TLMA and its theoretical age (Table 2).

Taking into account the slow spreading rates and the visible position of the basement in seismic profile showing the general symmetry of its deepening in a range from the walls of the rift valley toward the basins to LMA 13ny, we can conclude that a determination error of its position has occurred.

The attempt at the LMA 13ny identification [65, 93, 94] in the eastern part of the EB from retrospective domestic aeromagnetic data characterizing by low density of network and large navigation errors is important. The eastern part differs in low spreading rates [2] that intensify the effect of MAF superposition from single chrons. If we consider the MAF curves [65, 93] above the interpreted seismic profile, it is noteworthy that the local MAF, which can be identified as LMA 13n, is absent on the curves.

Sedimentary Sequence EB-4

The above located sedimentary sequence EB-4 reflects the changes that occurred after the beginning of a new evolution stage of the EB (Figs. 9a, 9c, 10). In the Nansen and Amundsen basins, the top overlaps the oceanic basement with a theoretical age of ~18.6 and 19.2 Ma, respectively. By its position, the top is correlated with the reflector of ~17.5 Ma, which is recognized in the western part of the Amundsen Basin and related to the beginning of the oceanic phase in the EB [44].

Some features of this sequence could be shown on the example of the interpretation of the reflector that overlaps the oceanic basement of the Nansen and Amundsen basins with theoretical ages of ~24.5 and ~19.6 Ma, respectively, and divides this sedimentary sequence into two subsequences, EB-4A and EB-4B (Figs. 9a, 9c).

This reflector is recognized in the western part of the Amundsen Basin and, in comparison with LMA, its age is estimated at <25–20 Ma [44]. The clear age inconsistency of this reflector in the Amundsen and

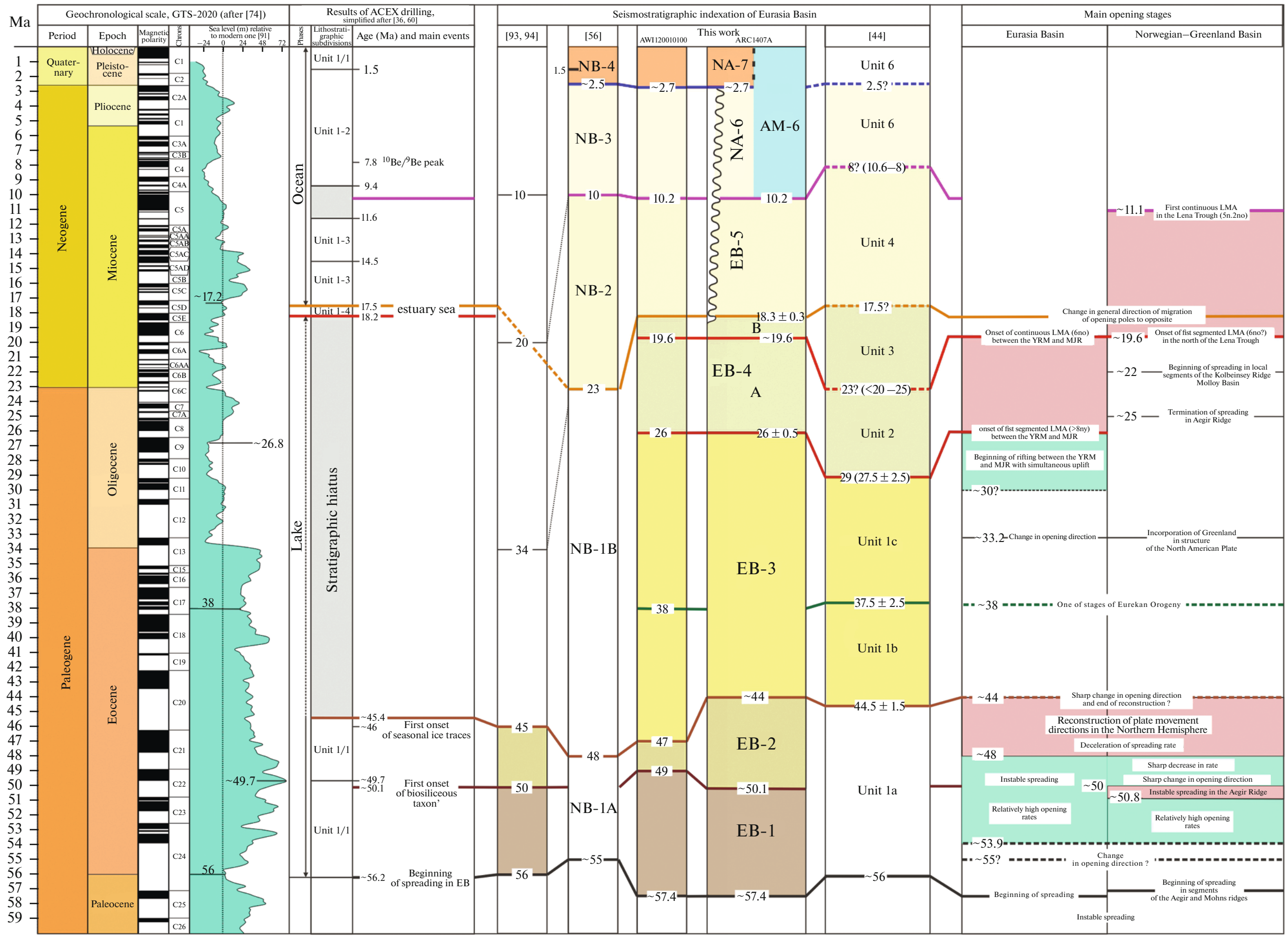

Fig. 10. The scheme of seismostratigraphic correlation of sediments along the line of profile ARC1407A and its correlation with drilling results of the ACEX boreholes and main tectonic stages of the evolution of the Norwegian–Greenland and Eurasia basins after [2, 9, 16, 36, 42, 44, 49, 55, 56, 60, 62, 64–66, 69, 70, 93].

Nansen basins revealed in this work indicates a previous tectonic event, which was identified by mutual location of sedimentary cover with the oceanic crust in the Amundsen Basin (Figs. 9a, area A).

The tops of sedimentary subsequences EB-4A and EB-4B and other internal contrasting horizons are approximately parallel to the oceanic basement, which sharply dips to the north. If we compare this area with that of the present-day rift valley in the Amundsen Basin, the following analogs are clearly traced.

The distance from the center of the rift valley to the top of the wall is ~11 km and, according to the calculations, this oceanic crust area formed for over ~2.7 Ma. Taking the fact into account that the spreading rate slightly increases beginning from LMA 2An.3o (3.596 Ma) [12], it is logical to suggest that the segment in area A, which is ~9.4-km long and formed for approximately over ~1.5 Ma, is a relic of the wall of the paleorift valley, which underwent intense uplifting (Fig. 9a, area A).

This area within sedimentary subsequence EB-4B has intense reflections, which could be interpreted as sills intruding the sedimentary cover as a result of intense magmatic eruptions during the period of formation of this oceanic crust area in the rift valley, i.e., the age of the top of sedimentary subsequence EB-4B could be equal to the theoretical value in the Amundsen Basin of ~19.6 Ma (Fig. 9a, area A).

This period corresponds to the formation of the first continuous and intense LMA 6no anomalies between the Yermak Plateau and Morris Jessup Rise in the EB and the flanks of the Kolbeinsey Ridge in the Norwegian–Greenland Basin [2, 42, 62, 66, 89]. This reflector in the western part of the Nansen Basin corresponds to the top of layer NB-1B [56] in seismic profile AWI20010100 (Fig. 9b).

The age indexation of this reflector of 19.6 Ma fully coincides with the determination of age of the top of subsequence EB-4B (Figs. 9a–9c, 10).

The top of subsequence EB-4A is located slightly closer to the rift valley, i.e., its age (similarly to the interpretation of ARC1407A seismic profile) can be accepted as ~18.3 Ma (Figs. 9a, 9c).

Sedimentary Sequence EB-5

The top of sedimentary sequence EB-5 overlaps the oceanic basement of the Nansen and Amundsen basins at ~10.2 and ~13 Ma, respectively (Fig. 9a). The position of the top coincides with a reflector distinguished in [93], which is indexed at 20 Ma. In [93], the age was indexed by the position of LMA C6ny (~18.636 Ma), but the sharp asymmetry of distances from the center of the rift valley to this LMA in the Amundsen and Nansen basins (~77.5 and ~59 km, respectively) allows its erroneous recognition in the Nansen Basin (Figs. 9a, Table 2).

The top of sequence NB-2 corresponds to 10 Ma in the western part of the Nansen Basin [56] (Fig. 10).

Because of the dissection of the basement surface and the low thickness of sedimentary lenses in the near-rift depressions, it is impossible to trace the top of the sequence toward the rift valley (Fig. 9b). In [56], the age of the sequence is calculated on the basis of the analysis of sedimentation rates in comparison with results from the ACEX borehole [36, 37, 60]. By hypsometric level, sequence EB-5 in the Amundsen Basin corresponds to layer Unit-4 (17.5(?)–8(?) 10.6–8 Ma) [44], which is close to our theoretical age values. The age of the top of layer Unit-4 is correlated with a ^{10}Be-dated hiatus at a depth of 135.5–140.4 m in the ACEX drill core (after [60], recalibrated after [45]) and the onset of Fe–Mn crusts in the flank of the Lomonosov Ridge [84].

The age of top of sequence EB-5 of 10.2 Ma, in our opinion, remains the same as the TLMA position in the Nansen Basin, which corresponds to an insignificant stratigraphic hiatus over the period of 11.6–9.6 Ma, as was observed in the ACEX borehole [36, 37].

Sedimentary Sequences EB-6-NA, EB-7-NA, and EB-6-AM

The age indexation of the above located sequences with TLMA is difficult due to the dissected seafloor of the near-rift seamounts, preventing correct determination of the onlap point of the reflector on the oceanic basement. We interpreted the sequences as having an age of <10.2 Ma.

DISCUSSION

The Period of the Formation of Sedimentary Sequence EB-1 (54.7–50.1 Ma)

The beginning of the formation of the sequence is related to the beginning of the EB spreading, which is accepted as ~57.4 Ma. The age of the top of seismic sequence EB-1 is accepted as ~50.1 Ma, which totally coincides with previous results [93] (Fig. 10). One of the explanations of this boundary is related to its link with climate changes [93].

At the same time, there are evident tectonic factors. A jumplike decrease in the rate and a strong change in the direction of spreading (∟30°–40°) occurred at 50–48 Ma in the northeastern Atlantic [64], although the full spreading rates were relatively high at the period of 53.9–44.0 Ma in the EB: 2.2–2.7 cm/year [2]. The directions of transform zones in the Labrador Sea changed in the period of 50–48 Ma [64].

A semigraben, whose age is estimated at 55 Ma, is located in the Amundsen Basin north of the TLMA C24no (53.9 Ma) toward the Lomonosov Ridge within the entire local basement inlier (Fig. 9a). The work [92] suggested a change in the direction of spreading at its earliest stage in the EB. An inversion with the age of 53.5 ± 1 Ma was observed in the West Spitsbergen Fault Zone, which is related to the beginning of the transform displacement of Greenland relative to the northwestern part of the EB [104] and the beginning of the northward displacement of Greenland relative to North America [97]. The age of this event is estimated at ~55 Ma (Fig. 10).

The Period of the Formation of Sedimentary Sequence EB-2 (50.1–44.0 Ma)

The theoretical age of the top of the sedimentary sequence is ~44 and ~41.8 Ma for the Amundsen and Nansen basins, respectively. Because the theoretical age is slightly younger than the beginning of the stratigraphic hiatus (45.4 Ma) in the ACEX borehole [36, 37], we can assume a scenario of the earlier uplift of the central segment of the Lomonosov Ridge above sea level and erosion of a small part with an already formed sedimentary sequence.

It is possible that the younger age of the top of the sedimentary sequence EB-2 in the Nansen Basin is related to the reconstruction of the direction of plate movements in the Northern Hemisphere, which occurred during 47.7–43.5 Ma (Figs. 9, 10).

In addition to the change in the direction of the EB drift lines, the relics of this reconstruction are traced in seismic data. The deformation of the sedimentary cover located below the top of sequence EB-2 is observed in seismic data in front of the eastern part of the FJLA [93]. This indicates that the main change in the spreading direction in this part of the Nansen Basin occurred earlier than ~44 Ma.

Seismic profile ARC1407A for this age range contains no evident signatures of deformation in the sedimentary cover, but exhibits a clear local asymmetry of the basement surface in the nearest areas to the place of the reflector onlap. The local asymmetry includes a minor displacement of the theoretical age of the formation of oceanic crust in characteristic near-rift depressions of the Nansen and Amundsen basins (Figs. 9a, 9b, points B, B').

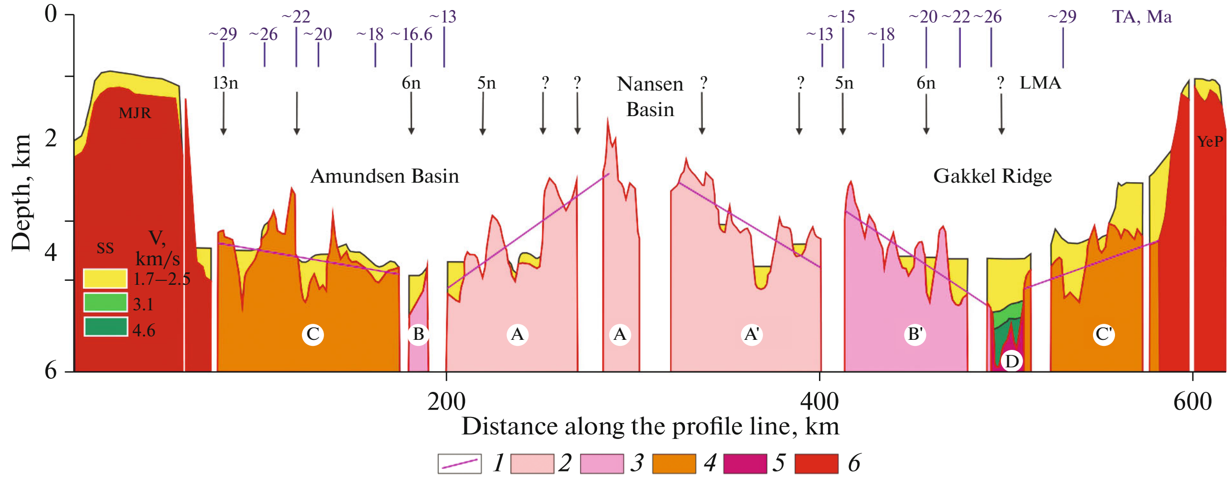

Fig. 11. Interpretation of seismic profile AWI-91, modified after [82]. For the position of the profile, see Fig. 1 (drift lines *6* and *8*). Abbreviations: YeP, Yermak Plateau; MJR, Morris Jessup Rise; SS, identified sedimentary sequences after [82]; LMA, identified linear magnetic anomalies after [82]; TA, theoretical age (Ma). A, A' and B, B', areas of symmetric deepening of the basement in the Amundsen and Nansen basins relative to the Gakkel Ridge; C, C', areas of symmetric uplift of the basement in the Amundsen and Nansen basins relative to the Gakkel Ridge; D, area of sharp deepening in the Nansen Basin without symmetric reflection in the Amundsen Basin. (*1*, regional trend of topography within (A, A'), (B, B'), (C, C'), and (D, D') segments; (*2*, *3*) types of oceanic crust formed during symmetric spreading (*2*) and asymmetric spreading (jump/jumps of opening axis (?)) (*3*); (*4*) continent–ocean transition zone (asymmetric rifting (?)); (*5*) oceanic crust formed during the beginning of spreading (D)(?); (*6*) continental crust.

This can indicate local jumps of the spreading axis, which are missed in calculations of the theoretical age of the oceanic crust based on symmetric spreading. The deviation of ~2 Ma shows the absence of a local jump component in the calculations for the Nansen Basin.

Global plate reorganization does not occur rapidly and if this is true ~2 Ma marks the duration of the local reconstruction in the EB and therefore the age of the formation of the top of sequence EB-2 within these limits.

The Period of the Formation of Sedimentary Sequence EB-3 (44–26 ± 0.5 Ma)

This sequence characterizes the complex interaction of three plates (Eurasian, North American, and Greenland) and peculiarities of sedimentary cover in the western part of the EB. The bottom and top of this sequence identified on ARC1407A seismic profile are clearly correlated with the reflector identified in the western part of the Nansen and Amundsen basins (Fig. 10).

Judging from the ARC1407A seismic profile within sequence EB-3, there are no objective reasons for its more detailed division. Two layers however are recognized in the western part of the Amundsen Basin in this period of [44]: Unit-1b (~44.5 ± 1.5–~37.5 ± 2.5 Ma) and Unit-1c (~37.5 ± 2.5–~27.5 ± 2.5 Ma). The reflector of 38 Ma is recognized in the western part of the Nansen Basin (Figs. 9, 10).

During 40–38 Ma, the direction of spreading in the Eurasia and Norwegian–Greenland basins changed [62, 64]. The full averaged spreading rates were also slow: ~1.8 cm/year (the initial stage of less than 50 Ma at ~3.8 cm/year) for the Norwegian–Greenland Basin [62] and ~1.5 cm/year (the initial stage of less than 50 Ma at ~2.5 cm/year) for the EB [2].

In this period, Greenland continued to move toward the north [97]. It is evident that the changes in the directions and spreading rates observed in the Norwegian–Greenland and Eurasia basins should be reflected symmetrically between the Greenland and North American plates, but these changes cannot correctly be observed due to extremely low spreading rates in the western part of North Atlantic.

The $^{40}Ar/^{39}Ar$ age of basaltic flows of the Ellesmere Island is 49–47 Ma and is accepted as a peak of Eurekan Orogeny in some works [109]. The age of 40–38 Ma reflects the later orogenic stage, which affected the northern areas of the Ellesmere Island and probably the Morris Jessup Rise and Yermak Plateau. These areas were the local provenances that supplied sediments during 44–38 Ma in the adjacent western part of the EB, but which are not traced to the eastern part.

As in [44], we accept a tectonic factor of the formation of the top of sequence EB-3 with the age of 26 Ma. This age corresponds to the termination of spreading in the Aegir paleoridge in the Norwegian–Greenland Basin.

New qualitative aeromagnetic data [70, 71] refine the age of termination of spreading, because the presence of LMA C12-11no (~30.6–30 Ma) nearest to the paleorift is reliably determined. The age of termination of spreading of ~25 Ma is determined assuming a systematic decrease in the ultraslow spreading rate, which occurred just after the period of the formation of C21r (47.760–48.878 Ma) [70, 71].

It is considered that the age of 27.5–26.0 corresponds to the formation of the first segmented LMA in the northern part of the segment between the Morris Jessup Rise and Yermak Plateau [42, 78]. If we index the age period with the geomagnetic polarity inversion scale, the interval corresponds to a period of frequent magnetic field inversions in the range of C8–C11 (~25–30 Ma) (Fig. 10).

In this period, the EB had low spreading rates [2], thus LMA identification is hampered because of the superposition of anomalous fields from some blocks of chrons of different polarity. In its geomorphological and geophysical characteristics, the segment between the Morris Jessup Rise and Yermak Plateau differs from the rest part of the EB [2] with only one transverse segmented profile AWI-91 conducted within its limits in 1991 (Figs. 6, 8).

The identification of the profile [82] was based on obsolete results of LMA identification of 1979 [111]; thus, we again indexed the seismic section with a theoretically calculated age emphasizing the clear asymmetry of the structure of the ridge flanks (Fig. 11). The description of the peculiarities of the structure of sedimentary cover is taken from [82].

Directly on the uplifts, the thickness of the sedimentary cover is only 100–200 m; there are erosion signatures. If we consider the regional principles of the basement topography from the present-day spreading center toward the flanks from the viewpoint of its subsidence with the increasing age of the formation of the oceanic crust, it occurs only in the central area, A–A' (Fig. 11) and is limited by the age of ~13 Ma for the Amundsen and Nansen basins, indicating symmetric spreading.

The maximum thickness of sediments in the depressions is ~200 m. The next area B' in the Nansen Basin has no counterpart in the Amundsen Basin, indicating unstable spreading during this period and jump/jumps of the spreading axis (Fig. 11). The maximum thickness of sediments in the depressions is ~400 m.

The next symmetric areas, B and B', in general plan (Fig. 11) exhibit an opposite change in regional directions increasing toward the slope foot. The basement topography allows their identification as areas of active rifting (continent–ocean transition zone (?)).

There is a deep graben in the Nansen Basin (area C) with a theoretical age of formation of 27–26 Ma, in which the maximum thickness of sediments is three times higher (~1500 m) in contrast to the opposite area in the Amundsen Basin (Fig. 11).

The lower part of the section strongly differs in higher seismic velocities (3.1 and 4.5 km/s), which can indicate active intrusion of basalts to sediments. This area can be interpreted as an initial spreading stage (?).

Because of the absence of significant jump/jumps of the spreading axis in area B and B', the theoretical age determination in area C and the next areas toward the rises are groundless, because they were based on general spreading symmetry (Fig. 11).

It is difficult to make theoretical calculations of the possible time of the jump because of the extremely curving single seismic profile in this segment of the EB (Figs. 6, 8).

We can suggest the following scenario. The initial stage of separation of the Morris Jessup Rise from the Yermak Plateau was accompanied by a regional uplift, which also affected the western part of the Lomonosov Ridge, the northern part of the Spitsbergen Archipelago, the north of the Ellesmere Island, and possibly the area between the Spitsbergen Archipelago and the FJLA (its western part?).

This is indirectly supported by the results of calculations of the Cenozoic uplift showing high values of the uplift for the northwestern part of the Barents Sea rather than for the northeastern, central, and southern parts [4, 75]. It is likely that a mantle plume was located beneath this area [42]; its traces occur at present as a local minimum in tomographic models [63] that defines the magmatic scenario of the evolution in this segment [48].

This is emphasized by the sharp AMF intensity [2], which is atypical of the entire EB area. Numerous traces of grabens are observed in seismic data on the Yermak Plateau [69], whereas intense magnetic anomalies [42] and contrasting local reflections in sedimentary cover [69] allow their interpretation as the intrusion of basalts during continental rifting.

The age of ~30 Ma can be accepted as the beginning of active rifting between the Yermak and Plateau and Morris Jessup Rise with the uplift of territories, which was followed by spreading in local segments at ~26 ± 0.5 Ma. A confident reflector of this age is thus distinguished from seismic data of the western part of the Amundsen Basin and the western part of the eastern sector of the EB.

The Period of the Formation of Sedimentary Sequence EB-4 (26 ± 0.5–18 ± 0.3 Ma)

Seismic sequence EB-4 is subdivided into two subsequences and has a series of specific signatures (Figs. 9a–9c, 10). By its hypsometric level, the lower subsequence EB-4A (26 ± 0.5–19.6 Ma) corresponds to layer Unit-2 (27.5 ± 2.5–23(?)) (<20–25) Ma [44] in the western part of the Amundsen Basin and is clearly correlated with the reflector in the western part of the Nansen Basin. After the termination of spreading in the Aegir Ridge at ~25 Ma [71], the first spreading segments of the further Kolbeinsey Ridge [40, 63] and Molloy Basin [55, 104], which divides the Knipovich Ridge from the Lena Trough, form with a minor delay during the formation of LMA 6B (~22 Ma).

LMA 6no (~19.6 Ma) is the first that was distinguished in the north of the Lena Trough and is continuously traced between the Morris Jessup Rise and Yermak Plateau [55]. The age of the top of EB-4 (~19.6 Ma) reflects the age of the fast phase of amalgamation of North Atlantic and EB.

The upper subsequence EB-4B (19.6–18.3 ± 0.3 Ma) corresponds to the top of layer Unit-3 (23 (?)) (<20–25)–17.5 (?) Ma [44]. In [44], the age of 17.5 Ma is correlated with the end of the estuary sea phase according to the results of the interpretation of the AXES borehole [36, 37].

The period of 18.636–18.007 Ma (LMA 6ny–5Ey) saw a fundamental reconstruction of spreading of the North Atlantic–EB system (Fig. 7). Beginning from the period of the formation of LMA 24no (53.9 Ma) to LMA 6ny (18.636 Ma), the main direction of migration of spreading poles occurred toward the NNW. Beginning from the period of LMA 5Ey (18.007 Ma), at least, before LMA 1no (0.773 Ma) and, probably, at present, the main direction of migration of the spreading pole reversed (SSE). It is thus logical to suggest that the formation of this boundary was a result of this reconstruction. Because there are no chrons of magnetic polarity between LMA 6ny and 5Ey, we can provide only the average probable estimation of the age of this event of ~18.3 ± 0.3 Ma, which indicates the beginning of the oceanic phase in the EB (Fig. 10).

The Period of the Formation of Sedimentary Sequences EB-4AM, EB-6-NA, and EB-7-NA

The upper sedimentary sequences younger than 10.2 Ma show striking asymmetry of thicknesses and the character of the seismic record in the Amundsen and Nansen basins (Fig. 9a, 9c). Four subsequences are distinguished within the Amundsen Basin in sedimentary sequence AM-6 by their seismic records (Fig. 9a). In [44], the upper part of the sediments is subdivided only into two layers Unit-5 (8 (?)–2.5 (?) Ma) and Unit-5 (2.5 (?)–0 Ma), in which the age of 2.5 Ma corresponds to the Late Pliocene–Quaternary glaciation stage of the Arctic [31]. The sharp dissection of the basement surface in the Amundsen Basin in the ARC1407A seismic profile prevents correct tracing of the reflector toward the Gakkel Ridge; thus we did not divide sequence AM-6 in more detail (Fig. 9a).

A striking feature of the sedimentary sequence within the Nansen Basin is related to the presence of areas of significant or partial loss of signal coherence (Fig. 9a, 9c, areas 1, 1'; 2, 2'; 3; 4, 4'; 5). The same areas are known in the western part of the Nansen Basin [9, 24, 56] and are interpreted as landslide bodies or intense turbidite flows (further, objects). In [56], similar objects occur within the sequences that formed from glaciomarine sediments of the Late Pliocene–Quaternary glaciation stage of the Arctic, as was established by deep-water drilling in the northern part in the Norwegian–Greenland Basin and on the Yermak Plateau [31, 95, 96].

The German, Norwegian [56], and Russian seismic profiles in the western part of the Nansen Basin were correlated in [9]. It has been established that the upper sequence of the sedimentary cover in the Russian seismic data, which hosts the objects, is identical to the sequence, as was determined in [56] as a Late Pliocene–Quaternary glaciomarine age with the lower boundary of ~2.5 Ma (2.7 Ma [74]).

In [56], sequence NB-4 was divided into two subsequences by the boundary of 1.5 Ma (Fig. 10). In our study, no more detailed division of sequence NA-7, which hosts landslide bodies, was conducted and the age of its foot was accepted as 2.7 Ma (Figs. 9a–9c, 10).

There is a significant difference in the thicknesses and lengths of glaciomarine sediments on profiles AWI-20010100 and ARC1407A (Figs. 9a, 9b). Seismic profile AWI-20010100 indicates that the glaciomarine sediments do not transit to the rift valley and stop before the near-rift seamounts. On the ARC1407A seismic profile, they are characterized by significantly higher thickness and the presence of a significant number of longer landslide bodies, which indicates the more intense contribution of sedimentary material. It can be stated that the age of sediments in the present-day rift valley of the Gakkel Ridge is less than 2.7 Ma, because it formed exactly during this period (Fig. 9a).

In the Norwegian–Greenland Basin, the maximum 3–4 km of the thickness of glaciomarine sediments, which comprise ~60% of the total thickness of the entire Cenozoic sediments [96], are observed in the area located in front of the Medvezhinsky Trough (Fig. 1) [31, 57]. Profile ARC1407A is located on a traverse of St. Anna and Voronin troughs, which together exceed the size of the Medvezhinsky Trough (Fig. 1).

Thawing waters and glaciomarine sediments were delivered to the central part of the Nansen Basin along the St. Anna and Voronin trenches. At the initial thawing stage of the ice cover, the intense mud flows led to sliding of previously formed slope sediments. The lower landslide bodies are submarine landslides of sedimentary cover formed during a period of <19.6–2.7 Ma, which partly eroded the upper part of sedimentary sequence EB-4B and completely eroded EB-5 and EB-6 (10.2–2.7 Ma) in a significant part of the Nansen Basin (Figs. 9a, 9b, areas 1, 1').

During further Quaternary thawing cycles of ice covers, the intensity of mud flows was high, thus they overflowed the rift valley of the Gakkel Ridge, as is similar to the interpretation results of seismic data of the Knipovich Ridge [32]. This overflow led to the origination of an uncertainty area of interrelations of sediments that were delivered to the Amundsen Basin from the Nansen Basin and directly formed in the Amundsen Basin (Fig. 9b, area B).

Profile ARC1407A within the rift valley of the Gakkel Ridge contains sediments ~600-m thick (Fig. 9a). The sedimentary sequences in the rift valley are observed on seismic profiles AWI20010300, ARC1405, ARC026, ARC024, ARC1216, and ARC1420 [79, 83] (Fig. 1). Beginning from profile AWI20010300, the seafloor of the rift valley becomes flatter toward the Laptev Sea (Fig. 6).

The narrowing of the EB is related to approaching to the spreading poles. The rift valley thus approaches the provenances of sediments: the Kara continental margin, which had ice cover, as suggested, during the Late Pliocene–Quaternary glaciation stage [23, 83, 95].

It is suggested that the sharp asymmetry of seafloor depths in the eastern part of the EB in the Nansen and Amundsen basins is related to the contribution of significant volumes of Late Pliocene–Quaternary glaciomarine sediments in the eastern part of the Nansen Basin, which also penetrate the rift valley of the Gakkel Ridge.

CONCLUSIONS

The following conclusions can be drawn as a result of our studies.

(1) The sedimentary sequences on seismic section ARC1407A and their stratigraphic indexation are close to those in the western parts of the Nansen and Amundsen basins.

(2) The age of sedimentary sequences corresponds to the ACEX drilling results and the main stages (onset, reconstruction, and deceleration of spreading) of the evolution of the Eurasia Basin.

(3) The reference horizon, which was previously recognized in the Eurasia Basin with the age of ~34 Ma related to the termination of spreading in the western part of North Atlantic and incorporation of Greenland Plate in structure of North American Plate, is not identified similarly to the results of study in the western parts of the Nansen and Amundsen basins.

(4) The reflector of ~38 Ma, which was earlier traced in the western part of the Amundsen Basin, was distinguished in the western part of the Nansen Basin. Its formation is related to one of the evolution stages of the Eurekan Orogeny of 40–38 Ma.

(5) The reflector of ~26 Ma, which was traced in the western part of the Amundsen Basin, is recognized in the western part of the Nansen Basin and within ARC1407A seismic profile. The origination of this extensive boundary is related to the beginning of unstable spreading in the western segment of the Eurasia Basin between the Yermak Plateau and Morris Jessup Rise.

(6) The termination of the long stratigraphic hiatus of 44.4–18.2 Ma in the ACEX section is clearly correlated with the origination of the sedimentary sequence of 19.6–18.3 Ma, which supports the beginning of the formation of a deep-sea gateway between the North Atlantic and Eurasia Basin. This event coincides with the main stage of the change in direction of movements of the Eurasian and North American plates, which is expressed in the change of the general direction of migration of momentary spreading poles from NNW to the SSE.

(7) Thick sedimentary sequences in the Nansen Basin and the rift valley of the Gakkel Ridge, which are observed on ARC1407A seismic profile, are Late Pliocene–Quaternary glaciomarine sediments (<2.7 Ma). Our research confirmed that the thick sediments studied in the Nansen Basin and the rift valley of the Gakkel Ridge comprise a significant volume of sediments in the eastern part of the Amundsen Basin and the Gakkel Ridge.

ACKNOWLEDGMENTS

We are grateful to the Russian Federal Geological Fund (Moscow, Russia) for the possibility of using of seismic data. We are also thankful to N.P. Chamov (Geological Institute, Russian Academy of Sciences, Moscow, Russia) and an anonymous reviewer for fruitful comments and Editor M.N. Shoupletsova (Geological Institute, Russian Academy of Sciences, Moscow, Russia) for careful editing.

FUNDING

This work was supported by the Russian Science Foundation, project no. 22-27-00578 "Newest and Present-Day Geodynamics of West Arctic: Evolution and Influence of Active Tectonic Processes on Structural Elements and Sedimentary Cover of Deep-Water Basins and Shelves."

CONFLICT OF INTEREST

The authors declare that they have no conflicts of interest.

REFERENCES

1. V. Yu. Glebovskii, A. V. Zaionchek, V. D. Kaminskii, and S. P. Mashchenkov, "Numerical databases and maps of potential fields of Arctic Ocean," in *The Russian Arctic: Geological History, Minerageneses, Environmental Geology*, Ed. by D. A. Dodin and V. S. Surkov (VNIIOkeangeologiya, St. Petersburg, 2002), pp. 134–141 [in Russian].
2. V. Yu. Glebovsky, V. D. Kaminsky, A. N. Minakov, S. A. Merkur'ev, V. A. Childers, and J. M. Brozena, "Formation of the Eurasia Basin in the Arctic Ocean as inferred from geohistorical analysis of the anomalous magnetic field," Geotectonics **40**, 263–281 (2006).
3. V. Yu. Glebovsky, A. A. Chernykh, V. D. Kaminskiy, V. V. Vasiliev, M. S. Korneva, A. V. Suhanova, A. G. Red'ko, and I. V. Iakovenko, "General results and future plans of magnitometric and gravimetric investigations in the Arctic Ocean," in *70 Years in the Arctic, Antarctic and the World Ocean*, Ed. by V. D. Kaminskiy, G. P. Avetisov, and V. L. Ivanov (VNII-

Okeangeologiya, St. Petersburg, 2018), pp. 196–208 [in Russian].

4. I. S. Gramberg, N. K. Evdokimova, and O. I. Suprunenko, "Catagenetic zoning and petroleum potential of the sedimentary cover of the Barents Sea shelf," Russ. Geol. Geophys. **42** (11–12), 1808–1820 (2001).
5. E. A. Gusev, "Geological structure of conjugation area of the Lomonosov Ridge and the continental margin of Laptev and East Siberian seas," Neftegaz. Geol. Teor. Praktika **6** (3), 1–12 (2011).
6. L. A. Daragan-Sushchova, O. V. Petrov, Yu. I. Daragan-Sushchov, D. I. Leont'ev, and I. N. Savel'ev, "History of formation of the Eurasian basin, the Arctic Ocean, based on seismic data," Regional. Geol. Metallogen., No. 84, 25–44 (2020).
7. R. M. Demenitskaya, A. M. Karasik, and Yu. G. Kiselev, "The structure of the Earth's crust in Arctic," in *The Geology of Sea and Ocean Floors. Proceedings of International Geological Congress, Reports of Soviet Geologists, Session XXII, New Deli, India* (Nauka, Moscow, 1964), pp. 114–121.
8. V. D. Dibner, Ya. Ya. Gakkel', V. M. Litvin, V. T. Martynov, and N. D. Shurgaeva, "Geomorphological map of the Arctic Ocean," in *Proceedings of Scientific Research Institute of Arctic Geology (NIIGA)* (Gosgeoltekhizdat, Moscow, 1965), vol. 143, pp. 341–345.
9. A. V. Zaionchek and S. A. Merkuriev, "New results of the identification of linear magnetic anomalies in the western part of the Nansen Basin and their use for the seismostratigraphic analysis," in *Proceedings of XXIV International Scientific Conference (School) on Marine Geology "Geology of Seas and Oceans"* (IO RAN, Moscow, 2021), vol. IV, pp. 70–74. https://doi.org/10.29006/978-5-6045110-7-7
10. A. V. Zaionchek, A. V. Soloviev, H. Brekke, and J. I. Faleide, "Assessment of the exhumation age of Triassic deposits of the Franz Josef Land Archipelago: Tectonic consequences," in *Proceedings of LIII Tectonic Meeting "Tectonics of Earth's Crust and Mantle: Fundamental Problems-2022," February 1–5, 2022, Moscow* (GEOS, Moscow, 2022), vol. 1, pp. 169–172.
11. A. M. Karasik, "Plate tectonics of the Eurasian Basin of the Arctic Ocean," in *Problems of Geology of the Earth Polar Regions*, Ed. by I. S. Gramberg, V. M. Lazurkin, M. G. Ravich, and B. V. Tkachenko (Nauchno-Issled. Inst. Geol. Arktiki, Leningrad, 1974), pp. 23–31.
12. A. M. Karasik, L. A. Savostin, and L. P. Zonenshain, "Parameters of lithospheric plate movement in the Eurasia Basin of the Arctic Ocean," Dokl. Akad. Nauk SSSR **273** (5), 1191–1196 (1983).
13. B. I. Kim and Z. I. Gleizer, "Sedimentary cover of the Lomonosov Ridge: Stratigraphy, structure, deposition history, and ages of seismic facies units," Stratigr. Geol. Correl. **15** (4), 401–420 (2007).
14. Yu. G. Kiselev, *Deep Geology of the Arctic Basin* (Nedra, Moscow, 1986) [in Russian].
15. D. V. Levin, S. M. Kryukov, and A. M. Karasik, "Aeromagnetic survey in the central segment of the Soviet Arctic," in *Aeromagnetic Survey in Geology*, Ed. by R. M. Demenitskaya (Gosgeoltekhizdat, Moscow, 1963), pp. 52–64 [in Russian].
16. L. I. Lobkovsky, M. V. Kononov, and E. V. Shipilov, "Geodynamic causes of the emergence and termination of Cenozoic shear deformations in the Khatanga–Lomonosov Fault Zone (Arctic)," Dokl. Earth Sci. **492**, 356-360 (2020). https://doi.org/10.31857/S2686739720050102
17. S. P. Mashchenkov, V. Yu. Glebovskii, E. D. Daniel, A. V. Zaionchek, and V. D. Kaminskii, "A new coordinated digital database on the potentialf and seafloor topography of the Arctic Basin. Theory and practice of offshore geophysical surveys," in *Proceedings to Jubilee Conference on the 50th Anniversary of Russian Marine Geophysics* (Okeangeofizika, Gelendzhik, 1999), pp. 160–161 [in Russian].
18. *The Evaluation of the Prospects of Oil and Gas Fields on Russia's Continental Shelf Beyond the 200-mile Zone* (MAGE, Murmansk, 2015) [in Russian].
19. V. A. Poselov, G. P. Avetisov, V. V. Butsenko, et al., "The Lomonosov Ridge as a natural extension of the Eurasian continental margin into the Arctic Basin," Russ. Geol. Geophys. **53** (12), 1276–1290 (2012).
20. P. V. Rekant and E. A. Gusev, "Sediments in the Gakkel Ridge rift zone (Arctic Ocean): Structure and history," Russ. Geol. Geophys. **57** (9), 1283-1287 (2016). https://doi.org/10.15372/GiG20160903
21. P. V. Rekant, D. I. Leont'ev, and E. O. Petrov, "Neotectonic stage of the Arctic Basin evolution: New ideas, timing and regional correlation," Regional. Geol. Metallogen., No. 81, 60–72 (2020).
22. P. V. Rekant, O. V. Petrov, and E. A. Gusev, "Model of formation of the sedimentary system of the Eurasian Basin, the Arctic Ocean, as a basis for reconstructing its tectonic evolution," Geotectonics **55** (5), 676–696 (2021). https://doi.org/10.31857/S0016853X21050064
23. G. E. Rozenbaum and N. A. Shpolyanskaya, "Arctic seas of Russia. Paleocryolithozone. Middle Pleistocene Cold Stage (250 kyr BP)," in *Geology and Mineral Resources of the Russian Shelf: Atlas*, Ed. by M. N. Alekseev (Nauchn. Mir, Moscow, 2004), sheets 3–17, 3–18 [in Russian].
24. S. Yu. Sokolov, E. A. Moroz, N. P. Chamov, and I. S. Patina, "Paleogene–Quaternary polyfacies sedimentary system of the Southern Nansen Basin," Lithol. Miner. Resour. **56**, 375–389 (2021). https://doi.org/10.31857/S0024497X21050050
25. V. E. Khain, *Tectonics of Continents and Oceans* (Nauchn. Mir, Moscow, 2001) [in Russian].
26. A. A. Chernykh and A. A. Krylov, "Duration, causes and geodynamic significance of the Mid-Cenozoic hiatus in sedimentation at the near-pole part of the Lomonosov Ridge (based on IODP-302-ACEX Data)," Oceanology **57** (5), 675–684 (2017). https://doi.org/10.7868/S0030157417050094
27. E. V. Shipilov and V. A. Vernikovsky, "The Svalbard–Kara plates junction: Structure and geodynamic history," Russ. Geol. Geophys. **51** (1), 58–71 (2010).
28. E. V. Shipilov, L. I. Lobkovsky, S. I. Shkarubo, and T. A. Kirillova, "Tectono-geodynamic settings in the conjugation zone of the Lomonosov Ridge, Eurasian

Basin, and Eurasian continental margin," Geotectonics **55** (5), 655–675 (2021).

29. A. A. Shreider, "Linear magnetic anomalies in the Arctic Ocean," Okeanologiya **44**, 7668–777 (2004).
30. A. A. Shreider, A. L. Brekhovskikh, A. E. Sazhneva, M. S. Klyuev, Kh. Galindo-Zaldivar, I. Ya. Rakitin, "Geochronology of the Eurasian Basin floor," Protsessy Geosredakh **31** (1), 1504–1511 (2022).
31. N. Alexandropoulou, M. Winsborrow, K. Andreassen, A. Plaza-Faverola, P-A. Dessandier, R. Mattingsdal, N. Baeten, and J. Knies, "A Continuous seismostratigraphic framework for the Western Svalbard–Barents Sea margin over the last 2.7 Ma: Implications for the Late Cenozoic glacial history of the Svalbard–Barents Sea ice sheet," Front. Earth Sci **9**, 656732 (2021). https://doi.org/10.3389/feart.2021.656732
32. I. M. H. Amundsen, M. Blinova, B. O. Hjelstuen, R. Mjelde, and H. Haflidason, "The Cenozoic western Svalbard margin: Sediment geometry and sedimentary processes in an area of ultraslow oceanic spreading," Mar. Geophys. Res **32**, 441–453 (2011). https://doi.org/10.1007/s11001-011-9127-z
33. O. B. Andersen, "The DTU10 Gravity field and Mean sea surface," in *Proceedings of Second International Symposium of the Gravity Field of the Earth (IGFS2)* (Fairbanks, Alaska. 2010). https://www.space.dtu.dk/english/research/scientific_data_and_models/global_marine_gravity_field
34. O. B. Andersen and P. Knudsen, "DNSC08 mean sea surface and mean dynamic topography models," J. Geophys. Res. **114** (C11001), (2009). https://doi.org/10.1029/2008JC005179
35. O. B. Andersen, P. Knudsen, and P. Berry, "The DNSC08GRA global marine gravity field from double retracked satellite altimetry," J. Geodesy **84** (3), 191–199 (2010). https://doi.org/10.1007/s00190-009-0355-9
36. J. Backman, M. Jakobsson, M. Frank, F. Sangiorgi, H. Brinkhuis, C. Stickley, M. O' Regan, R. Lovlie, H. Palike, D. Spofforth, J. Gattacecca, K. Moran, J. King, and C. Heil, "Age model and core-seismic integration for the Cenozoic ACEX sediments from the Lomonosov Ridge," Paleoceanography **23**, 1–15 (2008). https://doi.org/10.1029/2007PA001476
37. J. Backman and K. Moran, "Expanding the Cenozoic paleoceanographic record in the Central Arctic Ocean: IODP Expedition 302 Synthesis," Central Europe J. Geosci. **1** (2), 157–175 (2009). https://doi.org/10.2478/v10085-009-0015-6
38. J. Backman, K. Moran, D. B. McInroy, L. A. Mayer, et al., *Proceedings of the Integrated Ocean Drilling Program. Expedition 302* (IODP Management Int., Edinburgh, 2006). https://doi.org/10.2204/iodp.proc.302.2006
39. G. Balmino, N. Vales, S. Bonvalot, and A. Briais, "Spherical harmonic modeling to ultra-high degree of Bouguer and isostatic anomalies," J. Geodes. **86** (7), 499–520 (2012). https://doi.org/10.1007/s00190-011-0533-4
40. A. Blischke, C. Gaina, J. R. Hopper, G. Peron-Pinvidic, B. Brandsdottir, P. Guarnieri, Ö. Erlendsson, and K. Gunnarsson, "The Jan Mayen microcontinent: An update of its architecture, structural development and role during the transition from the Ægir Ridge to the Mid-Oceanic Kolbeinsey Ridge," in *The NE Atlantic Region: A Reappraisal of Crustal Structure, Tectonostratigraphy and Magmatic Evolution* (Spec. Publ.—Geol. Soc. London, 2011, Vol. 447), pp. 1–40. https://doi.org/10.1144/SP447.5
41. S. Bonvalot, G. Balmino, and A. Briais, M. Kuhn, A. Peyrefitte, N. Vales, R. Biancale, G. Gabalda, F. Reinquin, and M. Sarrailh, *World Gravity Map*, Ed. by BGI-CGMW-CNES-IRD, (Commission for the Geological Map of the World, Paris, 2012). https://bgi.obs-mip.fr/activities/projects/world-gravity-map-wgm/.
42. J. M. Brozena, V. A. Childers, L. A. Lawver, L. M. Gahagan, R. Forsberg, J. I. Faleide, and O. Eldholm, "New aerogeophysical study of the Eurasian Basin and Lomonosov Ridge: Implications for basin development," Geology **31** (9), 825–828 (2003).
43. S. C. Cande and D. V. Kent, "Revised calibration of the geomagnetic polarity timescale for the Late Cretaceous and Cenozoic," J. Geophys. Res. **100**, 6093–6095 (1995). https://doi.org/10.1029/94JB03098
44. C. F. Castro, P. C. Knutz, J. R. Hopper, and T. Funck, "Depositional evolution of the western Amundsen Basin, Arctic Ocean: Paleoceanographic and tectonic implications," Paleoceanogr. Paleoclimatol. **33** (2018). https://doi.org/10.1029/2018PA003414
45. J. Chmeleff, F. von Blanckenburg, K. Kossert, and D. Jakob, "Determination of the ^{10}Be half-life by multicollector ICP-MS and liquid scintillation counting," Nucl. Instrum. Methods Phys. Res., Sect. B **268** (2), 192–199 (2010). https://doi.org/10.1016/j.nimb.2009.09.012
46. A. N. Christensen and O. B. Andersen, "Comparison of satellite altimeter-derived gravity data and marine gravity data," in *EAGE Extended Abstracts of 77th EAGE Conference and Exhibition. June 1–5, 2015, Madrid, Spain* (Europ. Assoc. Geosci. Eng., Vol. 2015), pp. 1–5. https://doi.org/10.3997/2214-4609.201412986
47. A. N. Christensen and O. B. Andersen, "Comparison of satellite altimetric gravity and ship-borne gravity—Off-shore Western Australia," in *ASEG Extended Abstracts of 25th International Conference and Exhibition "Interpreting the Past, Discovering the Future"* (J. ASEC, Vol. 16, no. 1, 2016), pp. 1–5. https://doi.org/10.1071/ASEG2016ab242
48. H. J. B. Dick, J. Lin, and H. Schouten, "An ultraslow-spreading class of ocean ridge," Nature **426**, 405–412 (2003).
49. A. Dossing, J. Hopper, A. Olesen, and J. Halpenny, "New aerogeophysical results from the Arctic Ocean, north of Greenland: Implications for Late Cretaceous rifting and Eurekan compression," Geochem. Geophys. Geosyst. **14** (10), 4044–4065 (2013).
50. A. Døssing, T. M. Hansen, A. V. Olesen, J. R. Hopper, T. Funck, "Gravity inversion predicts the nature of the Amundsen Basin and its continental borderlands near Greenland," Earth Planet. Sci. Lett. **408**, 132–145

(2014).
https://doi.org/10.1016/j.epsl.2014.10.011

51. S. S. Drachev, N. Kaul, and V. N. Beliaev, "Eurasia spreading basin to Laptev Shelf transition: Structural pattern and heat flow," Geophys. J. Int. **152**, 688–698 (2003).
52. S. S. Drachev and S. I. Shkarubo, "Tectonics of the Laptev Shelf, Siberian Arctic," in *Circum-Arctic Lithosphere Evolution,* Ed. by V. Pease and B. Coakley (Spec. Publ.—Geol. Soc. London, 2018, Vol. 460), pp. 263–283.
https://doi.org/10.1144/sp460.15
53. B. Ehlers and W. Jokat, "Subsidence and crustal roughness of ultra-slow spreading ridges in the northern North Atlantic and the Arctic Ocean," Geophys. J. Int. **177** (2), 451–462 (2009).
54. Ø. Engen, O. Eldholm, and H. Bungum, "The Arctic plate boundary," J. Geophys. Res. **108** (B2), 1–17 (2003).
https://doi.org/10.1029/2002JB001809
55. Ø. Engen, J. I. Faleide, and T. K. Dyreng, "Opening of the Fram Strait gateway: A review of plate tectonic constraints," Tectonophysics **450**, 51–69 (2008).
56. Ø. Engen, J. A. Gjengedal, J. I. Faleide, Y. Kristoffersen, and O. Eldholm, "Seismic stratigraphy and sediment thickness of the Nansen Basin, Arctic Ocean," Geophys. J. Int. **176**, 805–821 (2009).
57. J. I. Faleide, A. Solheim, A. Fiedler, and K. Vanneste, "Late Cenozoic evolution of the Western Barents Sea–Svalbard continental margin," Global Planet. Change **12** (1–4), 53–74 (1996).
https://doi.org/10.1016/0921-8181(95)00012-7
58. J. I. Faleide, E. Vdgnes, and S. T. Gudlaugsson, "Late Mesozoic–Cenozoic evolution of the South-Western Barents Sea in a regional rift-shear tectonic setting," Mar. Petrol. Geol. **10**, 186–214 (1993).
59. R. Forsberg and S. Kenyon, "Gravity and geoid in the Arctic region—the northern polar gap now filled," in *Proceedings of GOCE Workshop 2004. ESA-ESRIN Frascati, Italy* (ESA Publ. Division, Noordwijk, Norway, 2004). http://earth.esa.int/workshops/goce04/goce_proceedings/57_forsberg.pdf.
60. M. Frank, J. Backman, M. Jakobsson, K. Moran, M. O'Regan, J. King, et al., "Beryllium isotopes in Central Arctic Ocean sediments over the past 12.3 million years: Stratigraphic and paleoclimatic implications," Paleoceanography **23**, PA1S02, 1–12 (2008).
https://doi.org/10.1029/2007PA001478
61. T. Funck, J. Shimeld, and M. H. Salisbury, "Magmatic and rifting-related features of the Lomonosov Ridge, and relationships to the continent–ocean transition zone in the Amundsen Basin, Arctic Ocean," Geophys. J. Int. **229** (2), 1309–1337 (2022).
https://doi.org/10.1093/gji/ggab501
62. C. Gaina, L. Gernigon, and P. J. Ball, "Palaeocene-Recent plate boundaries in the NE Atlantic and the formation of the Jan Mayen microcontinent," J. Geol. Soc. London **166**, 601–616 (2009).
63. C. Gaina, S. Medvedev, T. H. Torsvik, I. Koulakov, and S. C. Werner, "4D Arctic: A glimpse into the structure and evolution of the Arctic in the light of new geophysical maps, plate tectonics and tomographic models," Surv. Geophys. **35**, 1095–1122 (2014).
https://doi.org/10.1007/s10712-013-9254-y
64. C. Gaina, A. Nasuti, G. S. Kimbell, and A. Blischke, "Break-up and seafloor spreading domains in the NE Atlantic," in *The NE Atlantic Region: A Reappraisal of Crustal Structure, Tectonostratigraphy and Magmatic Evolution,* Ed. by G. Peron-Pinvidic, J. R. Hopper, M. S. Stoker, C. Gaina, J. C. Doornenbal, and T. Funck (Spec. Publ.—Geol. Soc. London, 2017, Vol. 447), pp. 393–417.
65. C. Gaina, A. M. Nikishin, and E. I. Petrov, "Ultraslow spreading, ridge relocation and compressional events in the East Arctic region—a link to the Eurekan orogeny?" Arktos, No. 16, 1–17 (2015).
https://doi.org/10.1007/s41063-015-0006-8
66. C. Gaina, W. R. Roest, and R. D. Muller, "Late Cretaceous–Cenozoic deformation of northeast Asia," Earth Planet. Sci. Lett., No. 197, 273–286 (2002).
67. C. Gaina, S. Werner, R. Saltus, and S. Maus, "Circum-Arctic mapping project: New magnetic and gravity anomaly maps of the Arctic," Geol. Soc. London, Mem. **35**, 39-48 (2011).
https://doi.org/10.1144/M35.3
68. J. S. Gee and D. V. Kent, "Source of oceanic magnetic anomalies and the geomagnetic polarity timescale, in *Treatise on Geophysics*, Ed. by G. Schubert (Elsevier, Amsterdam, Belgium, 2007), pp. 455–507.
https://doi.org/10.1016/B978-044452748-6.00097-3
69. W. H. Geissler, W. Jokat, and H. Brekke, "The Yermak Plateau in the Arctic Ocean in the light of reflection seismic data—Implication for its tectonic and sedimentary evolution," Geophys. J. Int. **187** (3), 1334–1362 (2011).
https://doi.org/10.1111/j.1365-246X.2011.05197.x
70. L. Gernigon, A. Blischke, A. Nasuti, and M. San, "Conjugate volcanic rifted margins, seafloor spreading, and microcontinent: Insights from new high-resolution aeromagnetic surveys in the Norway Basin," Tectonics **34**, 1–27 (2015).
https://doi.org/10.1002/2014TC003717
71. L. Gernigon, D. Franke, L. Geoffroy, C. Schiffer, G. R. Foulger, and M. Stoker, "Crustal fragmentation, magmatism, and the diachronous opening of the Norwegian–Greenland Sea," Earth-Sci. Rev. **206**, 102839 (2019).
https://doi.org/10.1016/j.earscirev.2019.04.01110.1016
72. V. Yu. Glebovsky, L. C. Kovacs, S. P. Maschenkov, and J. M. Brozena, "Joint compilation of Russian and US Navy aeromagnetic data in the Central Arctic Seas," Polarforschung **68** (A), 35–40 (2000).
73. F. M. Gradstein, J. C. Ogg, M. D. Smith, and G. M. Ogg, *The Geologic Time Scale—2012* (1st ed.), Ed. by F. M. Gradstein, J. C. Ogg, M. D. Smith, and G. M. Ogg (Elsevier Sci. Oxford, UK, 2012).
74. F. M. Gradstein, J. G. Ogg, M. D. Schmitz, and G. M. Ogg, *The Geologic Time Scale—2020* (1st ed.), Ed. by F. M. Gradstein, J. C. Ogg, M. D. Smith, and G. M. Ogg, (Elsevier Sci. Oxford. UK, 2020).
75. E. Henriksen, H. Bjørnseth, T. Hals, T. Heide, T. Kiryukhina, O. Kløvjan, G. Larssen, A. Ryseth,

K. Rønning, and K. Sollid, "Uplift and Erosion of the Greater Barents Sea: Impact on Prospectivity and Petroleum Systems," Geol. Soc. London, Mem. **35** (1), 271–281 (2011).

76. M. Jakobsson, J. Backman, B. Rudels, J. Nycander, M. Frank, L. Mayer, W. Jokat, F. Sangiorgi, M. O' Regan, H. Brinkhuis, J. King, and K. Moran, "The early Miocene onset of a ventilated circulation regime in the Arctic Ocean," Nature **447**, 986–990 (2007). https://doi.org/10.1038/nature05924

77. M. Jakobsson, L. A. Mayer, C. Bringensparr, et al., "The International Bathymetric Chart of the Arctic Ocean. Version 4.0," Sci. Data **176** (7) (2020). https://doi.org/10.1038/s41597-020-0520-9

78. W. Jokat, P. Lehmann, D. Damaske, and J. B. Nelson, "Magnetic signature of North-East Greenland, the Morris Jesup Rise, the Yermak Plateau, the central Fram Strait: Constraints for the rift/drift history between Greenland and Svalbard since the Eocene," Tectonophysics **691** Pt. A, 98–109 (2016). https://doi.org/10.1016/j.tecto.2015.12.002

79. W. Jokat and U. Micksch, "Sedimentary structure of the Nansen and Amundsen basins, Arctic Ocean," Geophys. Rev. Lett. **31** (2), 1–4 (2004). https://doi.org/10.1029/2003GL018352

80. W. Jokat, J. O'Connor, F. Hauff, A. P. Koppers, and D. P. Miggins, "Ultraslow spreading and volcanism at the eastern end of Gakkel Ridge, Arctic Ocean," Geochem. Geophys. Geosyst. **20**, 1–19 (2019). https://doi.org/10.1029/2019GC008297

81. W. Jokat, G. Uenzelmann-Neben, Y. Kristoffersen, and T. M. Rasmussen, "Lomonosov Ridge—a double-sided continental margin," Geology **20**, 887–890 (1992).

82. W. Jokat, E. Weigelt, Y. Kristoffersen, et al., "New geophysical results from the south-western Eurasian Basin (Morris Jesup Rise, Gakkel Ridge, Yermak Plateau) and the Fram Strait," Geophys. J. Int. **123**, 601–610 (1995).

83. J. Knies, J. Matthiessen, C. Vogt, J. S. Laberg, B. O. Hjelstuen, M. Smelror, E. Larsen, K. Andreassen, T. Eidvin, and T. O. Vorren, "The Plio-Pleistocene glaciation of the Barents Sea—Svalbard region: a new model based on revised chronostratigraphy," Quat. Sci. Rev. **28** (9), 812–829 (2009). https://doi.org/10.1016/j.quascirev.2008.12.002

84. C. Knudsen, J. R. Hopper, P. R. Bierman, M. Bjerager, T. Funck, P. F. Green, J. R. Ineson, P. Japsen, C. Marcussen, S. C. Sherlock, and T. B. Thomsen, "Samples from Lomonosov Ridge place new constraints on the geological evolution of Arctic Ocean," Spec. Publ.—Geol. Soc. London **460**, 397–418 (2018).

85. L. C. Kovacs, V. Yu. Glebovsky, S. P. Maschenkov, and J. M. Brozena, "New map and grid of compiled magnetic anomalies from the Arctic Ocean," AGU Fall Meet. Abstr. **83** (47), 1330 (2002).

86. Y. Kristoffersen, *Eurasia Basin*, in *The Geology of North America*. Vol. L. *The Arctic Ocean Region,* Ed. by A. Grantz, L. Johnson, and J. F. Sweeney (GSA, Boulder, CO, USA, 1990), pp. 365–378.

87. S. P. Maschenkov, V. Yu. Glebovsky, and A. V. Zayonchek, "New digital compilation of Russian aeromagnetic and gravity data over the North Eurasian Shelf," Polarforschung **69**, 35–39 (2001).

88. K. J. Matthews, K. T. Maloney, S. Zahirovic, S. E. Williams, M. Seton, and R. D. Muller, "Global plate boundary evolution and kinematics since the Late Paleozoic," Global Planet. Change **146**, 226–250 (2016).

89. S. Merkouriev and C. DeMets, "High-resolution Quaternary and Neogene reconstructions of Eurasia—North America plate motion," Geophys. J. Int. **198**, 366–384 (2014). https://doi.org/10.1093/gji/ggu142

90. P. J. Michael, C. H. Langmuir, H. J. B. Dick, et al., "Magmatic and amagmatic seafloor generation at the ultraslow-spreading Gakkel ridge, Arctic Ocean," Nature **423** (6943), 956–961 (2003). https://doi.org/10.1038/nature01704

91. K. G. Miller, J. V. Browning, W. J. Schmelz, R. E. Kopp, G. S. Mountain, and J. D. Wright, "Cenozoic sea-level and cryospheric evolution from deep-sea geochemical and continental margin records," Sci. Advances **20**, eaaz1346, (2020). https://doi.org/10.1126/sciadv.aaz1346

92. A. Minakov, J. I. Faleide, V. Yu. Glebovsky, and R. Mjelde, "Structure and evolution of the northern Barents—Kara Sea continental margin from integrated analysis of potential fields, bathymetry and sparse seismic data," Geophys. J. Int. **188** (1), 79–102 (2012). https://doi.org/10.1111/j.1365-246X.2011.05258.x

93. A. M. Nikishin, C. Gaina, E. I. Petrov, et al., "Eurasia Basin and Gakkel Ridge, Arctic Ocean: Crustal asymmetry, ultraslow spreading and continental rifting revealed by new seismic data," Tectonophysics **746**, 64–82 (2018).

94. A. M. Nikishin, E. I. Petrov, S. Cloetingh, N. A. Malyshev, A. F. Morozov, H. W. Posamentier, V. E. Verzhbitsky, S. I. Freiman, E. A. Rodina, K. F. Startseva, and N. N. Zhukov, "Arctic ocean mega project: Paper 2—Arctic stratigraphy and regional tectonic structure," Earth-Sci. Rev. **217**, 1–59 (2021). https://doi.org/10.1016/j.earscirev.2021.103581

95. E. Larsen, K. H. Kjær, I. N. Demidov, S. Funder, K. Grsfjeld, M. Houmark-Nielsen, et al., "Late Pleistocene glacial and lake history of northwestern Russia," Boreas **35**, 394–424 (2006).

96. A. P. E. Lasabuda, N. S. Johansen, J. S. Laberg, J. I. Faleide, K. Senger, T. A. Rydningen, and A. Hanssen, "Cenozoic uplift and erosion of the Norwegian Barents Shelf—A review," Earth-Sci. Rev. **217**, 103609 (2021). https://doi.org/10.1016/j.earscirev.2021.103609

97. G. N. Oakey and J. A. Chalmers, "A new model for the Paleogene motion of Greenland relative to North America: Plate reconstructions of the Davis Strait and Nares Strait regions between Canada and Greenland," J. Geophys. Res. **117** (B10), 1–28 (2012). https://doi.org/10.1029/2011JB008942

98. J. Ogg, "Geovagnetic polarity time scale," in *The Geologic Time Scale—2020*, Ed. by F. M. Gradstein, J. G. Ogg,

M. D. Schmitz, and G. M. Ogg (Elsevier Sci. Oxford, UK, 2020), Ch. 5, pp. 159–192.

99. K. Piepjohn, W. V. Gosen, and F. Tessensohn, "The Eurekan deformation in the Arctic: An outline," J. Geol. Soc. London **173** (6), (2016). https://doi.org/10.1144/jgs2016-081

100. A. Poirier and C. Hillaire-Marcel, "Improved Os isotope stratigraphy of the Arctic Ocean," Geophys. Rev. Lett. **38** (14), 1–6 (2011). https://doi.org/10.1029/2011GL047953

101. C. W. Pontbriand, S. A. Soule, R. A. Sohn, S. E. Humphris, C. Kunz, H. Singh, K. Nakamura, M. Jakobsson, and T. Shank, "Effusive and explosive volcanism on the ultraslow-spreading Gakkel Ridge, 85°E," Geochem. Geophys. Geosyst. **13** (10), 1–22 (2012). https://doi.org/10.1029/2012GC004187

102. P. Rekant, N. Sobolev, A. Portnov, B. Belyatsky, G. Dipre, A. Pakhalko, V. Kaban'kov, and I. Andreeva, "Basement segmentation and tectonic structure of the Lomonosov Ridge, Arctic Ocean: Insights from bedrock geochronology," J. Geodynam. **128**, 38–54 (2019). https://doi.org/10.1016/j.jog.2019.05.001

103. D. T. Sandwell and W. H. Smith, "Global marine gravity from retracked Geosat and ERS-1 altimetry: Ridge segmentation versus spreading rate," J. Geophys. Res. Solid Earth **114**, 1978–2012 (2009).

104. N. W. Schaaf, P. T. Osmundsen, R. Van der Lelij, J. Schönenberger, O. K. Lenz, T. Redfield, and K. Senger, "Tectono-sedimentary evolution of the eastern Forlandsundet Graben, Svalbard," Norw. J. Geol. **100**, 1–39 (2021). https://doi.org/10.17850/njg100–4–4

105. S. B. Sekretov, "Structure and tectonic evolution of the Southern Eurasia Basin, Arctic Ocean," Tectonophysics **351** (3), 193–243 (2002). https://doi.org/10.1016/S0040-1951(01)00278-5

106. M. Seton, D. Müller, S. Zahirovic, C. Gaina, T. Torsvik, G. Shephard, A. Talsma, M. Gurnis, M. Turner, and S. Maus, "Global continental and ocean basin reconstructions since 200 Ma," Earth Sci. Rev. **113**, 212–270 (2012).

107. M. Seton, R. D. Muller, S. Zahirovic, S. Williams, N. Wright, J. Cannon, J. Whittaker, K. Matthews, and R. McGirr, "A global dataset of present-day oceanic crustal age and seafloor spreading parameters," Geochem. Geophys. Geosyst. **21**, e2020GC009214 (2020). https://doi.org/10.1029/2020GC009214

108. A. M. Tebenkov and A. N. Sirotkin, "A new occurrence of Cenozoic (?) basalt from Manbreen, Ny Friesland, Northeastern Spitsbergen," Polar Res. **8**, 295–298 (1990). https://doi.org/10.1111/j.1751-8369.1990.tb003 92.x

109. C. Tegner, M. Storey, P. M. Holm, S. Thorarinsson, X. Zhao, C.-H. Lo, and M. F. Knudsen, "Magmatism and Eurekan deformation in the High Arctic Large Igneous Province: ^{40}Ar–^{39}Ar age of Kap Washington Group volcanics, North Greenland," Earth Planet. Sci. Lett. **303** (3), 203–214 (2011). https://doi.org/10.1016/j.epsl.2010.12.047

110. USGS Earthquake Catalog. https://earthquake.usgs.gov/earthquakes/.

111. P. R. Vogt, P. T. Taylor, L. C. Kovacs, and G. L. Johnson, "Detailed aeromagnetic investigation of the Arctic Basin," J. Geophys. Res. **84**, 1071–1089 (1979).

Translated by I. Melekestseva